Catalysis Science & Technology

Recent Applications of Nickel and Nickel-based Bimetallic Catalysts for Hydrodeoxygenation of Biomass-derived Oxygenates to Fuels

Journal:	*Catalysis Science & Technology*
Manuscript ID	CY-ART-07-2022-001179.R2
Article Type:	Paper
Date Submitted by the Author:	13-Oct-2022
Complete List of Authors:	Yu, Xinbin; University of South Carolina, Williams, Christopher; University of South Carolina, Chemical Engineering

Recent Applications of Nickel and Nickel-based Bimetallic Catalysts for Hydrodeoxygenation of Biomass-derived Oxygenates to Fuels

Xinbin Yu[1] and Christopher T. Williams[1]*

[1]Department of Chemical Engineering, University of South Carolina, Columbia, SC 29208 USA

*Correspondence: willia84@cec.sc.edu

Abstract

The hydrodeoxygenation (HDO) of biomass-derived oxygenates to fuels is an effective way to reduce the negative environmental impact resulting from dependence on fossil energy. However, the complexity in the feedstock compositions (*e.g.* acids, phenols, esters) and the presence of large amount of water, present significant challenges to the design of HDO catalysts. Nickel and nickel-based bimetallic catalysts have been extensively investigated for HDO due to their high activity and low price over the past years. Lots of valuable information about the structure of catalysts (*e.g.* active sites, synergy among various sites) and HDO reactions (*e.g.* reaction routes, kinetics) has been found. In this mini-review, we first summarize the preparation methods of nickel and nickel based bimetallic catalysts and the strategies to improve the HDO performance. The mechanisms and kinetics on HDO of typical oxygenates (aromatic oxygenates, furanic compounds, carboxylic acids and esters) over different catalysts are compared to reveal how the synergistic effects among different functionalities enhance the HDO performance. Solvent effects, the mutual influence among oxygenates and HDO of raw feedstocks over nickel and nickel-based bimetallic catalysts are discussed as well. Finally, we recommend several directions for further research in nickel and nickel-based bimetallic catalysts for HDO reactions.

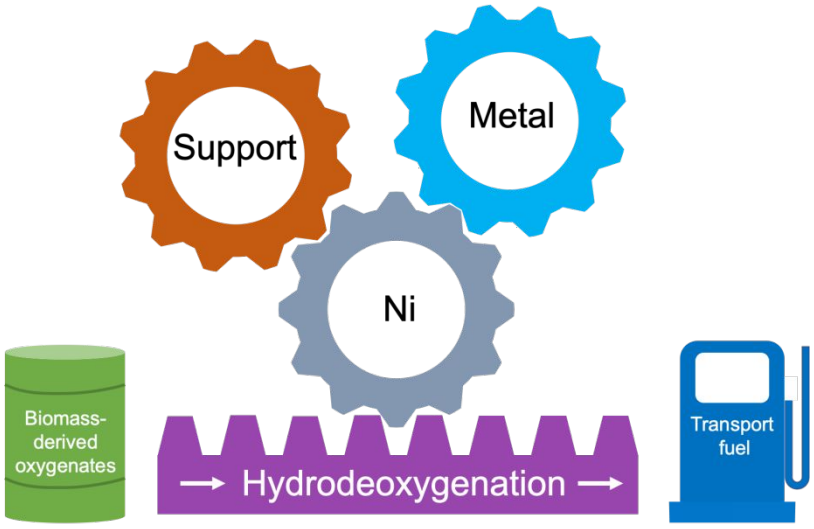

KEYWORDS: bio-oil, bio-fuel, oxygenates, hydrodeoxygenation, nickel catalysts, bimetallic catalysts

1. Introduction

Fossil fuels (*e.g.* petroleum, coal, natural gas) account for more than 80% of the primary energy demand, which provides a solid foundation for the energy needs of society.[1] However, the concomitant problems, such as the alarming rise of CO_2 level in the atmosphere and environmental pollution (*e.g.* smog, acid rain), compel us to reduce the dependence on fossil energy. Unlike fossil fuels, which are ancient plant and animal residues, biomass is a renewable organic material. The global biomass production is approximately 100 billion tons per year and the appropriate utilization of biomass derivatives can partly substitute fossil energy and mitigate those problems.[2,3]

Liquid biofuels mainly consist of bio-ethanol, bio-oils and bio-diesels. Bio-oils are typically produced from the abundant and cheap lignocellulosic biomass (**Figure 1** (A-C), *e.g.* wood, forest residues, and agricultural crops) *via* fast pyrolysis. In this process, biomass organic matrix is thermally decomposed in non-oxidizing atmospheres with high heating rates (up to 10^4 °C/s) and short residence times of solids (0.5-10 s, typically <2s), yielding liquid bio-oil, solid biochar, and gas fractions *via* a series of reactions such as dehydration, dehydrogenation/aromatization and carbonization.[4,5,6] It is estimated that energy density of biomass can be increased by a factor of 6-10 through fast pyrolysis.[7,8] The pyrolysis bio-oil contains hundreds of organic compounds (**Figure 2**) and the physical and chemical properties

are dramatically different from liquid fossil fuels (**Table 1**). The presence of a large amount of oxygen-containing compounds causes severe problems, such as instability of fuel quality, low heating value, high corrosiveness and high viscosity, which make bio-oil incompatible with existing engines.[9] To enhance the chemical properties of bio-oil, hydrodeoxygenation (HDO) is proposed, which uses H_2 to remove oxygen atoms primarily in the form of H_2O and produce hydrocarbons, through the catalytical cleavage of C-O bond at high temperatures (300-400 °C).[10]

The first-generation biodiesel is a mixture of fatty acid methyl esters (FAMEs) (**Figure 1** (D)) produced *via* transesterification. In this process, triglycerides react with methanol in the presence of alkali catalyst to form fatty acid methyl esters (FAMEs) and glycerol.[11,12] Although FAMEs are compatible with existing diesel engines and can be blended with fossil fuels, the low chemical and thermal stabilities and poor cold-flow properties restrict their applications (*e.g*. blending ratio).[13,14,15,16] The second generation biodiesel are typically produced from non-edible feedstock. Hydrodeoxygenation is also applied to remove the oxygen in FAMEs and fatty acid and obtain long chain alkanes.[17,18,19,20,21]

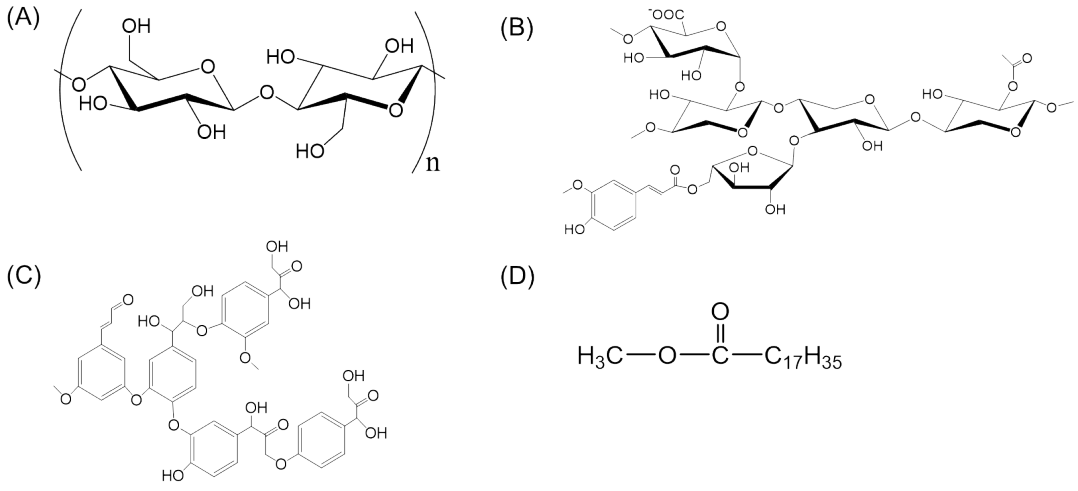

Figure 1. Structure of lignocellulose components (A) cellulose, (B) hemicellulose and (C) lignin; structure of bio-diesel component (D) FAME (alkyl= $C_{17}H_{35}$).

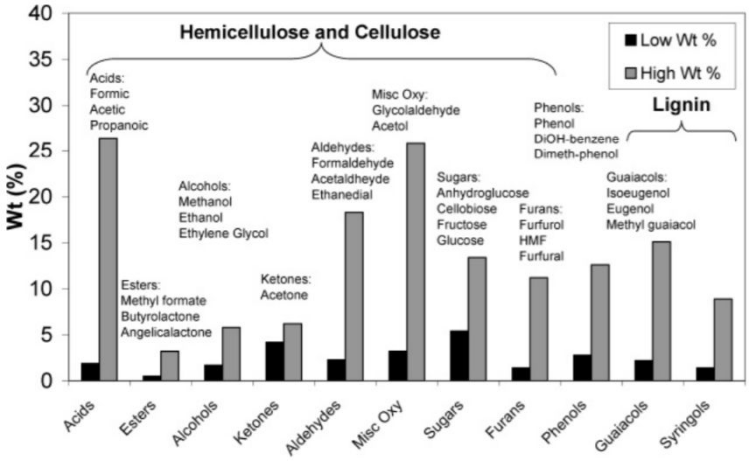

Figure 2. Chemical composition of bio-oil from wood biomass and its most abundant molecules. (Reproduced from ref. 22 with permission from American Chemical Society. Copyright 2006.)

Table 1. Physical properties of wood fast pyrolysis bio-oils and heavy fuel oil.[23,24]

Physical properties	Typical bio-oil	Heavy fuel oil
Moisture content, wt%	15-30	0.1
pH	2-3	-
Density (15 °C), kg/dm^3	1.10–1.30	0.99-0.995
C, wt %	54-58	85
H, wt %	5.5-7.0	11
O, wt %	35-40	1.0
N, wt %	0-0.2	0.3
S, wt %	below 0.05	1.0 (max)
Ash, wt%	0.01–0.1	0.08 (max)
HHV, MJ/kg	16-19	40
viscosity (at 50 °C), cP	40-100	180
solids, wt %	0.2-1	1
distillation residue, wt %	up to 50	1
Flash point, °C	40–110	65 (min)
Pour point, °C	-9–36	15 (max)
Stability	Unstable	-

Supported metal catalysts are usually employed to catalyze hydrodeoxygenation reactions. To take advantage of the existing hydroprocessing facilities, conventional hydrotreating catalysts, such as sulphided $CoMo/Al_2O_3$ and $NiMo/Al_2O_3$, are extensively studied. However, sulfided catalysts have problems, including requiring addition of sulfur in the process and subsequent leaching of sulfur into the products, low resistance to water, and coke deposition.[25] Noble metal catalysts (*e.g.* Pt, Pd, Ru, Rh) are also frequently employed for

hydrodeoxygenation, but their high cost and limited reserves significantly restricts the wide applications. Among all the supported non-noble metal catalysts, Ni-based catalysts have been extensively investigated due to their high activity and low price.[26,27,28]

Nickel catalysts are widely used in hydrogenation-related processes as Ni has exceptional capability of dissociating and chemisorbing H_2.[29,30,31] However, nickel catalysts are also very active for undesired reactions in HDO, such as C-C hydrogenolysis, ring saturation and methanation, which lowers the selectivity to target products and increases the consumption of H_2 in many cases. Hence, different strategies have been proposed to tune the properties of nickel catalysts, such as the incorporation of various elements (*e.g.* metals, phosphorous) and employing different supports. Moreover, the preparation methods of supported nickel-based catalysts often influence their performance in the hydrodeoxygenation reaction.

Several excellent reviews on the hydrodeoxygenation of biomass derived oxygenates with different emphasis have been published.[10,22,32] For example, Furimsky and Elliott discussed the detailed mechanisms and kinetics of HDO mainly over hydroprocessing catalysts and noble metal catalysts.[33,34] Wang *et al.* reviewed HDO of bio-oils and the individual model compounds over noble metal catalysts.[35] Kim *et al.* summarized the active sites requirements for HDO catalysts (mainly noble metal catalysts) and recent advances in electrochemical HDO processes.[36] The scope of this mini-review focuses on the preparation of supported nickel and nickel-based bimetallic catalysts and their applications in the hydrodeoxygenation of typical biomass derived oxygenates to fuels.

2. Preparation of nickel and nickel-based bimetallic catalysts

Table 2. Literature survey of Ni and Ni-based bimetallic catalysts for HDO of biomass derived oxygenates

Catalysts	Preparation methods	Reactants	Reactor	Performance (Conversion and selectivity to major products over catalysts at given conditions; yield is declared separately)	Ref.

10 wt% Ni/Silicalite-1	*in situ* encapsulation	Phenol	Flow reactor	71.2% (X_{phenol}), 99.2% (benzene) over Ni@Silicalite-1, 400 °C, 0.25 MPa H_2, m_{cata} = 1.0 g, phenol flowrate: 0.1 mL/min, H_2 flow rate: 300 mL/min.	37
5 wt% Ni/SiO_2	Precipitation−deposition; incipient wetness impregnation	m-Cresol	Flow reactor	95.6 % ($X_{m\text{-}Cresol}$), 67.6% (toluene), 11.6% (benzene) over 5wt%Ni/SiO_2 (1.8 nm), 300 °C, 0.1 MPa H_2, W/F = 6 h, 0.5 h reaction.	38
6.4 wt% Mo-46.6 wt% Ni/SiO_2-Al_2O_3	Hydrothermal coprecipitation	Phenol	Flow reactor	96% (X_{phenol}), ~ 90% (O-free products yield) over 6.4wt%Mo46.6wt%Ni/SiO_2-Al_2O_3, 310 °C, 3.0 MPa H_2, WHSV= 107.5 h^{-1}, TOS= 4 h.	39
12 wt%Ni-10 wt%Mo/SiO_2	Two-step incipient wetness impregnation	Phenol	Flow reactor	99.30 % (X_{phenol}), 99.27% (benzene), 410 °C, 0.1 MPa H_2, WHSV = 1.5 h^{-1}, H_2/substrate (mol/mol) = 5, 1 h reaction.	40
5 wt % Ni/SiO_2 modified with 9 wt % Fe, 16 wt % Mo, 30 wt % W	Incipient wetness impregnation	p-Cresol	Batch reactor	~96% ($X_{p\text{-}Cresol}$), ~52% (methylcyclohexane), ~27% (toluene), ~19% (4-methylcyclohexanol) over 5wt%Ni16wt%Mo/SiO_2, 60 mL of n-hexadecane 0.18 g of p-cresol, 0.2 g of a passivated catalyst, 250 °C, 1 MPa H_2, 2h reaction.	41
5 wt% NiNi/Hierarchical mesoporous ZSM-5	Incipient wetness impragenation	Anisole	Batch reactor	98 % ($X_{anisole}$), 84.2 % (cyclohexne), 15.4 % (methoxycyclo-hexane) over Ni/HSZ-c, 200 °C, 6.8 MPa H_2, 0.30 g of catalyst, 4.5 wt% anisole-n-decane (50 mL), 140 min reaction.	42
37 wt% Ni/Al_2O_3	Calcination and reduction of NiAl layered double hydroxide precursors	Anisole	Flow reactor	100 % ($X_{anisole}$), ~78% (cyclohexyl methyl ether), ~19% (cyclohexane) over Ni/Al_2O_3 (Ni/Al molar ratio = 1). 240 °C, 2 MPa H_2, H_2/oil (volume ratio) = 300, W/F = 0.45 min.	43
Ni-based hydrotreating catalyst	Commercially available	Anisole	Flow reactor	100 % ($X_{anisole}$), ~22 wt% (benzene) ~10 wt% (toluene), ~25 wt% (phenol), ~22 wt% (cresol) over Ni-based catalyst A. 350 °C, 0.17 MPa H_2, WHSV = 1.9 h^{-1}.	44
85 wt%Ni-5 wt%Cu/SiO_2	Decomposition and impregnation	Anisole	Batch reactor	100 %($X_{anisole}$),~85%(methoxycyclohexane), ~12% (cyclohexane) over 85wt%Ni5wt%Cu/SiO_2, 280 °C, 6 MPa H_2, 1 g of catalyst, 6 wt% anisole-hexadecane (50 ml), 13 min reaction.	45
4 wt%Ni-10 wt%Mo/SBA-15	Wet impregnation	Anisole	Flow reactor	62% ($X_{anisole}$), ~47% (methoxycyclohexane), ~17% (cyclohexne), ~14% (benzene) over NiMo/SBA-15, 250 °C, 1.5 MPa H_2, 250 mg of catalyst, H_2 flowrate = 100 ml/min.	46
10 wt%Ni-4 wt%Ga/SiO_2	Impregnation	Anisole	Flow reactor	71.8 % ($X_{anisole}$), 86.4% (benzene) over Ni_3Ga/SiO_2. 300 °C, 0.1 MPa H_2, WHSV = 1 h^{-1}, H_2/anisole molar ratio =25.	47
16 wt% Ni/Al-SBA-15	Incipient wetness impregnation	Eugenol	Batch reactor	100% ($X_{eugenol}$), ~78% (propyl cyclohexane), ~20% (gas products) over 16 wt%Ni/Al-SBA-15-E, 240 °C, 2 MPa H_2, 0.05 g of catalyst, 770 µL guaiacol, 40 mL dodecane, 680 rpm, 2h reaction.	48
0.56 wt% Ni/N-doped carbon molecular sieve	Thermal ionic-exchange	Vanillin	Batch reactor	58% ($X_{vanillin}$), ~100% (2-methoxy-4-methyl-phenol) over HD-Ni/NCMS (Ni: 0.56 wt%), 130 °C, 2 MPa H_2, reactant to catalyst molar ratio = 300, 1 h reaction.	49
40 wt% Ni/Red mud	Wet impregnation	Guaiacol	Batch reactor	83.2 % ($X_{guaiacol}$), 34.8% (cyclohexane), 23.1% (benzene), 16.6 % (toluene), 9.5% (phenol) over 40 wt%Ni/RM, 350 °C, 6.21 MPa H_2, 4.5 g of catalyst, 30 g of guaiacol, 30 min reaction.	50
18.1 wt% Ni/SiO_2	Ammonia evaporation method	Guaiacol	Batch reactor	100 % ($X_{guaiacol}$), ~95% (2-methoxycyclohexanol), ~4% (cyclo-hexanol) over 18.1 wt% Ni/SiO_2-AEH, 140 °C, 3 MPa H_2, 0.05 g of catalyst, 0.10 g guaiacol, 20 mL decalin, 5 h.	51

6.5 wt% Ni/BEA	Ion-exchange-deposition-precipitation	Guaiacol	Flow reactor	~11% ($X_{guaiacol}$), ~53% (cyclohexane), ~47% (other products) over 6.5 wt% Ni/BEA-IDP, 230 °C, 4 MPa H_2, 0.05 g of catalyst, guaiacol (0.156 g/min), H_2(120 mL/min), 40 min reaction,	52
5 wt% Ni-15 wt% Co/γ-Al_2O_3	Impregnation	Guaiacol	Batch reactor	100 % ($X_{guaiacol}$), ~58 % (cyclohexanol), ~13 % (1-methyl-1,2-cyclohexanediol, trans-), ~23 % (1-methyl-1,2-cyclohexanediol, cis-) over 5 wt%Ni15 wt%Co/γ-Al_2O_3, 200 °C, 5 MPa H_2, 5 g of guaiacol, 45 g of water, 1.02 g of catalyst, 8 h reaction.	53
10 wt% Ni-20 wt% Mo/Al_2O_3–TiO_2	Sol–gel process and spray pyrolysis method	Guaiacol	Flow reactor	100 % ($X_{guaiacol}$), ~86 % (cyclohexane), ~12 % (met-cyclohexane) over 10wt%Ni20wt%Mo/Al_2O_3–TiO_2, 300 °C, 2 MPa H_2, H_2 flowrate = 60 ml/min, WHSV = 57 h^{-1}, 2 h reaction.	54
36.5 wt%Ni-2.3 wt% Cu/ZrO_2-SiO_2-La_2O_3	Sol–gel	Guaiacol	Batch reactor	75 % ($X_{guaiacol}$), ~39% (cyclohexane), ~30% (1-methylcyclohexane-1,2-diol), 13%(cyclohexanone) over 36.5wt%Ni2.3wt%Cu/ZrO_2-SiO_2-La_2O_3, 320 ◦C,17 MPa H_2, 1 g of catalyst, 30 ml of guaiacol, 1h reaction.	55
10 wt % Cu-10 wt % Ni/CeO_2-SiO_2	Deposition−coprecipitation	Vanillin	Batch reactor	96% ($X_{vanillin}$), ~85% (2-methoxy-4-methyl-phenol) over 10 wt %Cu10 wt %Ni/CeO_2-SiO_2, 150 °C, 2.5 Mpa H_2, 0.02 g of catalyst, 0.228 g of vanillin, 10 mL of water, 1000 rpm, 12h reaction.	56
40 wt% Ni/ZSM-5	Solid phase grinding	HMF	Batch reactor	90% (X_{HMF}), ~95% (DMF) over 40%Ni/ZSM-5, 180 °C, 0.25 MPa H_2, m_{cata} = 0.05 g, 1mmol HMF, 10 mL tetrahydrofuran (THF), 7 h reaction,	57
18.2 wt% Ni/ZrP	Ion exchange	HMF	Batch reactor	100% (X_{HMF}), ~70% (DMF) over Ni/ZrP, 240 °C, 5 MPa H_2, 0.1 g of catalyst, 0.25 g of HMF, 40 mL of THF, 500 rpm, 5h reaction.	58
5 wt% Ni/Hβ	Incipient wetness impregnation	BBM	Flow reactor	90% (yield of diesel alkanes) over 5 wt% Ni/Hβ, 230 °C, 6 MPa H_2, 1.8 g of catalyst, WHSV = 1.3 h^{-1}, H_2 flow rate: 120 mL/min,	59
2.4 wt% Ni/Co_3O_4	Hydrothermal method	HMF	Batch reactor	100% (X_{HMF}), 76% (DMF) over Ni/Co_3O_4, 130 °C, 1 MPa H_2, 0.1 g of catalyst, 0.25 g of HMF, 10 ml of THF, 24 h reaction.	60
36.1 wt% NiSi-phyllosilicate	Ammonia evaporation	HMF	Batch reactor	100% (X_{HMF}), 64.1% (DMF), 26.1% (DMTHF) over 36.1 wt% NiSi-phyllosilicate, 150 °C, 1.5 MPa H_2, 0.08 g of catalyst, 1.5g of HMF, 38 mL of 1,4-dioxane, 3 h reaction.	61
4.8 wt% Ni-5.2 wt% Cu/C	Solvothermal synthesis followed by dispersion	HMF	Flow reactor	100% (X_{HMF}), ~90% (DMF) over 4.8 wt% Ni-5.2 wt% Cu/C, 180 °C, 3.3 MPa H_2, HMF flowrate/m_{cata} = 1 g*min/mL,	62
5.1 wt% Ni-4.9 wt% Fe/C	Incipient-wetness impregnation	Furfural	Flow reactor	100% ($X_{furfural}$), 65.4% (MF) over 10wt% NiFe/C (Fe/Ni molar ratio = 1), 180 °C, 0.1 MPa H_2, m_{cata}/(fufural + H_2) flowrate = 20 min*g/g, H_2/furfural = 100.	63
5 wt%Cu-3wt%Ni /TiO_2	Impregnation	Furfural	Batch reactor	100% ($X_{furfural}$), ~60% (MF), ~33% (MTHF) over 5 wt%Cu3wt%Ni/TiO_2, 200 °C, 3.5 MPa H_2, 0.3 g of catalyst, 1 g of furfural, 25 mL of 1,4-dioxane, 8h reaction.	64
1.4 wt%Ni–15 wt%Co/C	Impregnation	HMF	Batch reactor	99.0% (X_{HMF}), 96% (DMF) over 15wt%Co1.4wt%Ni/C, 130 °C, 1 MPa H_2, 0.2 g of catalyst, 0.252 g of HMF, 10.0 mL of THF, 24 h reaction,	65
4.0 wt% Ni/Al_2O_3	Atomic layer deposition (ALD)	Oleic acid	Flow reactor	100% ($X_{Oleic\ acid}$), ~72% (C16-C18 alkanes), ~20% (C9-C15 alkanes) over 4.0 wt% Ni (ALD)/Al_2O_3, 340 °C, 3.0 MPa H_2, 2.0 g of catalyst, H_2/oil = 500, WHSV = 2.4 h^{-1}	66
5.5 wt% Ni/KIT-5	Impregnation	Palmitic acid	Batch reactor	95% ($X_{Palmitic\ acid}$), 60% (n-pentadecane), 38% (1-hexadecanol) over 5.5 wt% Ni/KIT-5, 280 °C, 5.2 MPa H_2, 0.1 g of catalyst, 39 mM of PA, 40 mL of n-dodecane, 6 h reaction.	18
10 wt% Ni/SiO_2–ZrO_2	Wet impregnation	Stearic Acid	Batch reactor	100% ($X_{Stearic\ Acid}$), ~63% (C18), ~37% (C17) over 10 wt% Ni/37(mol%)SiO_2–ZrO_2, 260 °C, 4 MPa H_2, 0.05 g of catalyst, 0.5 g of stearic acid, 100 mL of dodecane, 600 rpm, 24 h reaction,	67

5.6 wt% Ni-4.2 wt% Cu/ZrO_2	Impregnation	Stearic acid	Batch reactor	100% ($X_{stearic\ acid}$), 98% (n-heptadecane) over 5.6 wt% Ni-4.2 wt% Cu/ZrO_2, 350 °C, 4 MPa H_2, 0.5 g of stearic acid, 0.2 g of catalyst, 100 mL of n-dodecane, 600 rpm, 4h reaction.	[68]

Note: HMF: 5-hydroxy-methyl-furfural, DMF: dimethylfurfural, BBM: 5,5′-(butane-1,1-diyl)bis(2-methylfuran)

In classic catalysis theories, surface sites (*e.g.*, terrace, step, corner, and kink) with different abilities for adsorption and cleavage/formation of bonds account for the catalytic activity.[69,70] Supports are commonly employed to disperse metallic species and increase the concentration of these active sites. Functionalities of supports (acid/base sites, oxygen vacancies, *etc.*) may participate in the HDO reaction. The introduction of support also induces the interaction between supports and metal species in many cases, which provides new active sites for reactions.

Many methods are proposed to fabricate supported nickel catalysts as shown in **Table 2**. Impregnation is the simplest and most popular method to disperse active species onto solid supports. A typical process of impregnation involves dissolving metal salts in a solvent (*e.g.* water) and then mixing the solution with support followed by evaporating the solvent to deposit the active species onto support. This method is widely employed in the synthesis of nickel and nickel-based bimetallic catalysts for the hydrodeoxygenation of oxygenates from bio-oil.[40,71] Incipient wetness impregnation is widely used in which the amount of solution is equal to the volume of solvent that supports can adsorb.[72,73] Excess impregnation is also applied in several cases.[74] In this method, the solid phase is obtained by filtration of the mixture with excess amount of solvent when the adsorption of metal ions onto the support reaches equilibrium. It is much easier to achieve required loading amount of metals on the support via incipient wetness impregnation than excess impregnation while the dispersion of metals is usually higher over catalysts prepared by excess impregnation.

Hydrodeoxygenation reactions involve the cleavage of C-C bonds and C-O bonds, which exhibits structure sensitivity in many cases.[37,66,75,76,77,78,79] Thus, the dispersion of metal on the support is one of the important parameters of HDO catalysts. A high dispersion

of nickel species is usually found beneficial to the catalytic activity and/or selectivity.[38,80,81,82] However, typical supported Ni catalysts (*e.g.* Ni/Al_2O_3, Ni/SiO_2) prepared by impregnation method usually have particles with large sizes and broad size distribution. Various strategies have been taken to overcome this problem. It is found that properties of supports (*e.g.* specific surface area, pore size, surface functional group, *etc.*) often influence the dispersion of nickel on the catalysts.[83,84,85,86] The incorporation of ZrO_2 into CeO_2 formed ZrO_2-CeO_2 solid solutions and increased the pore volume (0.06 to 0.12-0.17 m^3/g) and surface area (18 to 31-51 m^2/g) of CeO_2, which facilitated the Ni dispersion.[87] The crystallite size of Ni was 11.0 nm on $Ni/ZrO_2{-}CeO_2(2:1)$ whereas it was 17.0 nm on Ni/CeO_2. The surface functional groups also have effects on the dispersion of metallic species. Due to the strong anchoring effect of surface N groups on porous nitrogen-doped carbon black (NCB), high dispersion of Ni species was obtained on Ni/NCB catalysts.[88] The relative atomic percentage of metallic Ni species increased from 3.8% to 15.6% as the surface nitrogen content increased from 0 to 4.38 % on the support. A relatively low dispersion of NiO on MCM-41 was due to the low interaction between NiO and the hydrophobic surface of the MCM-41 support. The introduction of coordinated Ti species into the hexagonal channel of MCM-41 enhanced the dispersion of NiO species although the specific surface area of Ti-MCM-41 (705 m^2/g) is much lower than that of MCM-41 (983 m^2/g).[84]

A secondary metal species (*e.g.* Fe, Co, Mo, W) has frequently been reported to promote the dispersion of supported nickel species, although the mechanisms are not clear yet.[39,79,89,90,91,92] Possible reasons are the dilution effect of the second metal on Ni in a certain loading range and/or the interaction between different metal species. By keeping the loading amount of Ni at 5 wt% and increasing the loading amount of Mo from 0 to 4.6 wt%, the Ni particle sizes measured by XRD decreased from 23 nm to 8 nm.[91] Similarly, the increase in loading amount of Fe (from 0 to 8wt%) caused a decrease in the average particle size (from 7 to 4 nm) over $FeNi/SiO_2$ catalysts with 8 wt% Ni.[93]

To compare the effectiveness of different preparation methods, 5 wt% Ni/Hβ catalysts were prepared by four methods that included impregnation, deposition-precipitation (DP), ion exchange/precipitation, and Ni nanoparticle deposition.[82] The deposition-precipitation method could load Ni species onto Hβ with the smallest particle size (2.5 nm) and the tightest particle size distribution (standard deviation: 0.7 nm) (**Figure 3**) as OH^- for the deposition of Ni^{2+} was generated slowly and homogeneously by the decomposition of urea in the solution. The dramatic decrease in micropore volumes (by 0.06 cm^3/g) of the sample prepared by DP suggested that certain amount of Ni species was deposited in the micropores of HBEA. Catalysts prepared by deposition-precipitation (DP), ion exchange/precipitation, and Ni nanoparticle deposition showed much stronger interaction between Ni species and support than the sample prepared by impregnation according to H_2-TPR results. As Ni could form complex with NH_3, ammonia evaporation hydrothermal method (AEH) was developed. Compared to Ni/SiO_2 catalysts (15.1 nm) prepared by impregnation (IMP), Ni nanoparticles on catalysts prepared by AEH were trapped tightly in a fibrous nickel phyllosilicate box which yielded highly dispersed Ni nanoparticles (4.8 nm) on the support after reduction.[51] Moreover, the density of Lewis acid sites induced by coordinatively unsaturated (Ni^{2+}) cations was as high as 108.6 μmol/g on Ni/SiO_2 prepared by AEH, whereas it could not be detected on samples synthesized by impregnation.

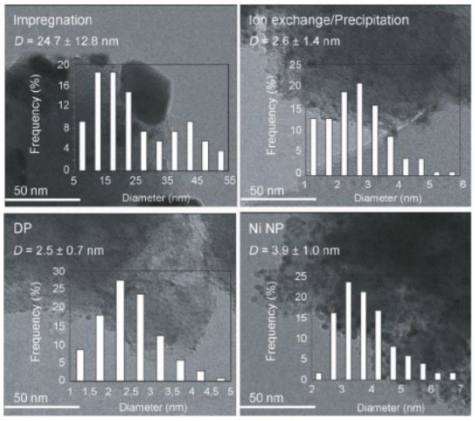

Figure 3. TEM images of reduced Ni/HBEA samples prepared by different methods; the respective insets are the histograms of Ni particle size distribution (after counting 300 particles). (Reproduced from ref. 82 with permission from Wiley-VCH Verlag GmbH & Co. KGaA, Weinheim. Copyright 2013.)

Calcination and reduction of Ni-containing layered double hydroxide (LDH) is a strategy that can yield catalysts with a good dispersion, uniform distribution of particle size and strong metal-support interaction. LDH structures can be synthesized by coprecipitation of several metal cations. With calcination and reduction at high temperature, the lamellar structure of LDH can undergo an *in-situ* topological structure transformation. Zhang *et. al.* prepared high loading (22 wt%-63wt%) Ni/Al_2O_3 catalyst by calcination and subsequent reduction of layered double hydroxide (LDH) precursors and found nickel species were homogeneously distributed on Al_2O_3.[43] The particle sizes measured by CO chemisorption ranged from 6.4 nm to 13.4 nm and the catalysts exhibited a mesoporous structure. The $Ni_{0.5}Zn_{1.5}Al_1$-LDH precursor showed a flower-like morphology with a 1-2 μm of flower-like structure.[94] Ni supported on mixed metal oxides (MMO) catalysts were obtained after calcination and reduction of NiZnAl-LDH precursors and the flower-like morphology was maintained. N_2 adsorption-desorption isotherms of the precursor and catalyst showed that they had meso/macropores. The BET surface area and pore diameters of $Ni_{0.5}Zn_{1.5}Al_1$ sample increased from 86 to 114 m^2/g and 12 and 18 nm after calcination and reduction, respectively. It was attributed to the collapse of LDH structure and loss of H_2O trapped in the LDH during the high temperature treatment.

Other preparation methods have also been explored to prepare supported nickel catalysts aiming to increase the dispersion of nickel species.[95,96] 10.6 wt % Ni@Silicalite-1 was prepared by hydrothermal encapsulation method. Ni nanoparticle sizes on the catalyst were 3−5 nm with a narrow distribution.[37] The significant drop (451.2 m^2/g to 272.2 m^2/g) in surface area of micropores of bare support suggested that encapsulation of Ni nanoparticles in the pores of Silicalite-1. As carbon support has very high specific surface area and rich surface functional groups, it can facilitate the dispersion of metal species. Ni@C catalysts were prepared by the pyrolysis of Ni-MOF.[97] The catalyst still maintained the spherical structure of MOF after high temperature (650 ^oC) treatment but the surface became rough. EDX results showed that the Ni species were uniformly dispersed on C. The high Ni loading induced rich medium acidic sites (46.87 mmol/g) on Ni@C-650 sample, which was beneficial to certain reactions. Besides, the high temperature treatment induced the reduction of NiO to Ni

by carbon matrix. 7.2 wt%WO_3-5 wt%Ni/C bimetallic catalysts were prepared by atomic layer deposition (ALD) of 5 wt%Ni/C.[72] The size of most Ni particles was in the range of 5-8 nm. Moreover, it was observed that WO_x species preferentially deposited on Ni particles rather than on the surface of C support, which facilitated the interaction between Ni and WO_x species.

However, small particle sizes sometimes induce too strong interactions between metallic sites and other species as well as between metallic sites and support, which subsequently decreases the catalytic activity.[78,98,99,100] Much attention should also be paid to the utilization of other functionalities (*e.g.* acidity) to achieve the synergy among different sites as HDO involves many parallel and sequential reactions, such as dehydration, cracking and hydrogenolysis.

3. HDO of Biomass-derived Oxygenates

The raw feedstocks (bio-oils and bio-diesels) contain different amounts of various oxygenates depending on process parameters and source of biomass. Typical oxygenates are furans, phenols, guaiacols, carboxylic acids and esters, and carbohydrates. Their oxygen-containing functional groups exhibit differences in reactivity, which pose difficulties in the elucidation of mechanisms using crude bio-oil. Hydrodeoxygenation of individual model compound is usually conducted to simplify the problem and obtain essential information about the reaction routes. Both the properties of catalysts and reaction conditions significantly influence the specific pathways.

3.1 HDO of Aromatic Oxygenates

Phenol and phenolic derivatives are abundant in bio-oil, representing the cellulose and lignin part in the lignocellulosic biomass. However, the p-Π conjugated interaction between aromatic ring and O atom elevates C-O bond strength (468 kJ/mol) and makes phenol and phenolic derivatives (*e.g.* phenol, anisole, guaiacol) among the most persistent oxygen-containing compound in bio-oil.

As the simple phenolic compounds, phenol and cresol are usually employed as model compounds for hydrodeoxygenation of bio-oil. The reaction routes are proposed to depend on the adsorption mode of phenol (*i.e.* co-planar and non-planar) on the surface.[89,101,102,103,104] The hydrogenation of phenol on nickel and nickel-based bimetallic catalysts at mild temperature (< 300 °C) primarily produces ring-hydrogenated products *via* several sequential reactions as shown in **Scheme 1.**[80,89,105,106,107]

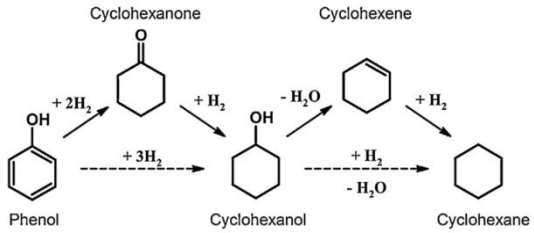

Scheme 1. Reaction scheme of HDO of phenol under mild conditions. Solid arrows indicate main pathways, while the dotted arrows indicate the steps of the kinetic model. (Reproduced ref. 80 with permission from Elsevier. Copyright 2016.)

The support materials significantly influence the catalytic performance of nickel catalysts in the HDO of phenol. A variety of Ni catalysts with different supports (ZrO_2, SiO_2, Al_2O_3 and C) for phenol hydrodeoxygenation were compared in a batch reactor.[106] The overall order of HDO activity followed $Ni/ZrO_2 > Ni\text{-}V_2O_5/ZrO_2 > Ni\text{-}V_2O_5/SiO_2 > Ni/Al_2O_3 > Ni/SiO_2 >> Ni/C$. Ni/ZrO_2 exhibited the best performance (full conversion of phenol and 80% yield of cyclohexane at 275 °C, 10 MPa of H_2, 1 g of catalyst in 50 g of phenol and 5 h reaction) due to the balanced reaction rates of hydrogenation and deoxygenation (**Figure 4**). Ni/C was active for HDO of cyclohexanol rather than phenol. The oxygen vacancies on the oxide support might play an important role in the activation and hydrogenation of phenol and Ni sites were responsible for the deoxygenation reaction. The rate determining step of phenol hydrodeoxygenation on Ni/ZrO_2 was dehydration of cyclohexanol because of the lack of acidity of ZrO_2. Higher acid site concentration (from 0 to 0.77 mmol/g) on Ni/HZSM-5 could increase the initial turnover frequency (from 127 to 769 h^{-1}) of phenol hydrodeoxygenation.[103] Zhao *et al.* found that the individual reaction steps on Ni/HZSM-5 and Ni/Al_2O_3-HZSM-5 followed the rate order r_1(phenol hydrogenation) < r_2(cyclohexanone hydrogenation) < r_3(cyclohexanol dehydration) << r_4(cyclohexene hydrogenation).[105] The incorporation of Al_2O_3 to Ni/HZSM-5 promoted the dispersion of

Ni from 2.5% to 8% which led to a significant increase in the catalytic activity for hydrogenation of phenol, cyclohexanone and cyclohexene over that of Ni/HZSM-5 (**Table 3**). Besides, the Lewis acidity induced by Al_2O_3 could stabilize ketone species. Higher content of Brønsted acidic sites and the synergy between acid sites and metal sites benefitted the dehydration of cyclohexanol and subsequent hydrogenation of cyclohexene.

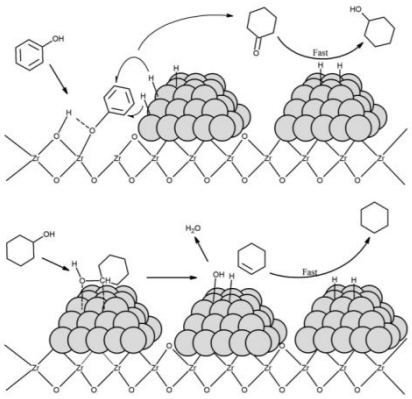

Figure 4. Proposed reaction mechanism for HDO of phenol over an oxide-supported nickel catalyst (here Ni/ZrO_2). Gray spheres represent nickel atoms. (Reproduced from ref. 106 with permission from American Chemical Society. Copyright 2013.)

Table 3. TOF and E_a data for aqueous-phase phenol hydrodeoxygenation reaction network at 200 °C on Ni catalysts. (Reproduced from ref. 105 with permission from Elsevier. Copyright 2012.)

Reaction	Ni/HZSM-5	Ni/Al_2O_3-HZSM-5
Step 1: Phenol hydrogenation		
r_1 (mmol g^{-1} h^{-1})	14	61
TOF_1 (mol $mol^{-1}_{Surf.Ni}$ h^{-1})	398	553
E_{a1} (kJ mol^{-1})	48	56
Step 2: Cyclohexanone hydrogenation		
r_2 (mmol g^{-1} h^{-1})	108	159
TOF_2 (mol $mol^{-1}_{Surf.Ni}$ h^{-1})	2443	1233
E_{a2} (kJ mol^{-1})	142	129
Step 3: Cyclohexanol dehydration		
r_3 (mmol g^{-1} h^{-1})	528	354
TOF_3 (mol mol^{-1}_{BAS} h^{-1})	7428	8333
E_{a3} (kJ mol^{-1})	112	114
Step 4: Cyclohexene hydrogenation		
r_4 (mmol g^{-1} h^{-1})	1813	2156
TOF_4 (mol $mol^{-1}_{Surf.Ni}$ h^{-1})	55,136	20,287
E_{a4} (kJ mol^{-1})	35	25

Although carbon support was not recommended for the HDO of phenol on nickel catalyst, Ni/mesoporous carbon spheres (MCS) catalysts were very active for HDO of phenol.[89] The hydrogenolysis of cyclohexanol to cyclohexane was the rate determining step. The performance could be further improved by incorporation of Fe onto Ni/MCS due to the formation of Ni-Fe alloy identified by X-ray powder diffraction

(XRD) and Mössbauer spectroscopy techniques , which provided more sites for the adsorption of cyclohexanol *via* oxygen and facilitated the hydrogenolysis of cyclohexanol. By varying the Ni/Fe ratio while keeping the total metal loading the same, the specific surface area, pores volume and pore size of catalysts were similar. XRD results revealed that increasing the loading amount of Fe could decrease the crystallite size. The amount of H_2 uptake also decreased as increasing the amount of Fe. The optimal Ni/Fe ratio was 3/1 and the synergy between metallic Ni sites and NiFe alloy sites were crucial for activation of H_2 and cleavage of C-O bond. Phenol conversion of 99.8%, cyclohexanol selectivity of 49.1%, and cyclohexane selectivity of 49.9% was obtained over $10Ni_3$-Fe_1/MCSs.[89,106]

Interest is growing in retaining the aromatic character of the upgraded oils as it can not only minimize the hydrogen consumption in the process but also increase the octane value of the fuel.[34] Thus, direct hydrogenolysis of the C_{Ar}-O bond is a preferred route and is also thermodynamically preferred over ring saturation.[81,108] However, hydrogenolysis of C_{Ar}-O bond is kinetically less favorable than hydrogenation of aromatic ring because of much weaker adsorption of hydroxyl compared to the strong adsorption of aromatic ring upon Ni catalysts. Achieving high selectivity to aromatic products usually requires high temperature to suppress the adsorption of aromatic ring.[109] Shi *et al.* prepared Ni@Silicate-1 catalyst *via in situ* encapsulation method and then applied it to the HDO of phenol.[37] Ni species were trapped within the channel of Silicate-1 to promote the adsorption of phenol *via* end-up mode (**Figure** 5), resulting in much higher selectivity (68%) to products from phenol hydrogenolysis than the counterparts (42% and 19%) on impregnated Ni/Silicate-1 and Ni/SiO_2 at low temperature (250 °C).

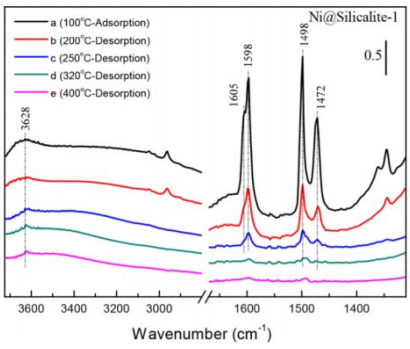

Figure 5. *In situ* FT-IR spectra analysis of phenol adsorption on Ni@ Silicalite-1 catalyst at different desorption temperatures. (Reproduced from ref. 37 with permission from American Chemical Society. Copyright 2019.)

The adsorption of hydroxyl could also be enhanced over oxophilic metal (Fe, Mo, *etc.*) and/or oxygen vacancies on supports (ZrO_2, TiO_2, Nb_2O_3, *etc.*) by strong interaction between oxygen atom and oxophilic sites.[110,111,112,113] Resende *et al.* dispersed nickel species onto $Ce_{1-x}Nb_xO_2$ support and found that suitable amount of niobium species (Nb/Ce: 0 to 2.3) increased the selectivity to benzene (from 8.38% to 86.92%) in the hydrodeoxygenation of phenol.[114] It was explained by that the incorporation of niobium promoted the formation of oxygen vacancies by changing the lattice parameter of ceria and enhanced the interaction between the oxygen of hydroxyl and the oxophilic sites. Bimetallic Ni-Mo/SiO_2 catalyst with Ni:Mo molar ratio ≈ 1 was very active and selective for HDO of m-cresol to toluene over 250−350 °C and 1 atm of H_2 (**Figure 6**).[91] The enhanced performance was ascribed to the decoration of Ni surface by reduced MoOx moieties. Hsu *et al.* compared the effect of oxophilic promoters (FeO_x, MoO_x, and WO_x) on the direct deoxygenation of *p*-cresol on Ni/SiO_2 (**Figure 7**).[41] The Ni/metal (Fe, Mo or W) molar ratio was kept around 0.5. XRD profiles verified the formation of NiFe, NiMo, NiW alloy and TEM results indicated that the particle sizes on three catalysts were similar (9-10 nm). Although the oxophilicity measured by metal−oxygen bonding strength followed the order of $FeO_x < MoO_x < WO_x$, it was NiMo/SiO_2 that generated highest toluene yield due to MoO_x species' moderate activity for direct deoxygenation and inertness to toluene hydrogenation at 250 °C and 1 MPa of H_2 pressure.

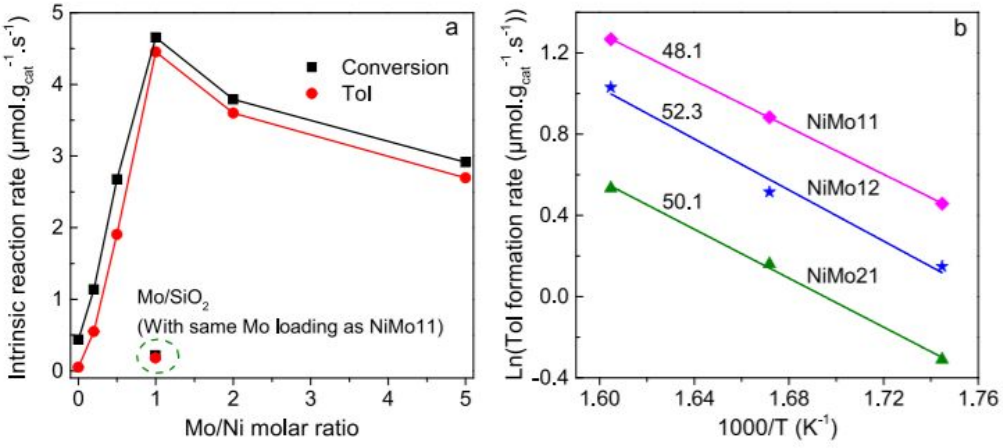

Figure 6. (a) Effect of Mo/Ni molar ratio on the intrinsic reaction rate of m-cresol conversion and Tol formation at 350 °C. (b) Arrhenius plots of m-cresol deoxygenation to Tol over NiMo catalysts with different Mo/Ni molar ratios at a temperature range of 300−350 °C. Number near the line shows the activation energy with units of kJ/mol. Reaction conditions: H_2/m-cresol = 60, P = 1 atm, TOS = 30 min. W/F was adjusted to achieve m-cresol conversion < 10%. NiMo11: Ni/Mo molar ratio=1:1, NiMo12: Ni/Mo molar ratio=1:2, NiMo21: Ni/Mo molar ratio=2:1. (Reproduced from ref. 91 with permission from American Chemical Society. Copyright 2019.)

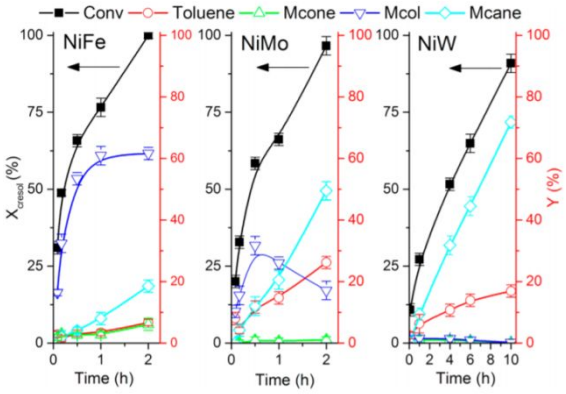

Figure 7. Conversion of *p*-cresol and yields of toluene, 4-methylcyclohexanone (Mcone), 4-methylcyclohexanol (Mcol), and methylcyclohexane (Mcane) as a function of time through tested catalysts at 250 °C, 1 MPa H_2 pressure, 60 mL of a solvent (n-hexadecane), 0.18 g of a reactant (p-cresol), and 0.2 g of a passivated catalyst in a 300 mL stirred batch autoclave. NiFe: 5 wt % Ni-9 wt % Fe/SiO_2, NiMo: 5 wt % Ni-16 wt % Mo/SiO_2, NiW: 5 wt % Ni-30 wt % W/SiO_2. (Reproduced from ref. 41 with permission from American Chemical Society. Copyright 2018.)

Anisole is used as a model compound for HDO because it represents the methoxy-rich aromatic molecules from the lignin in bio-oil. The primary reactions happening during the hydrodeoxygenation of anisole are the direct deoxygenation (hydrogenolysis of C_{Ar}-O bond), transalkylation (hydrogenolysis of C_{Methyl}-O bond), hydrogenation of aromatic ring and dehydration.[46,44,85] A typical reaction network is shown in **Scheme 2**.

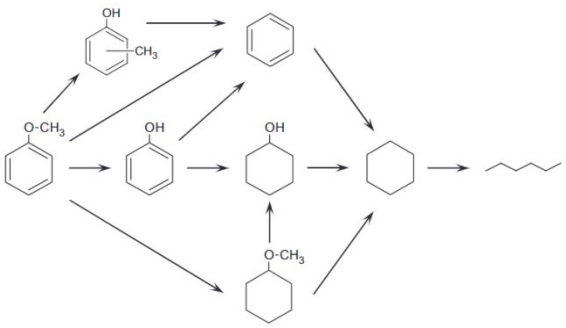

Scheme 2. Possible routes for anisole hydrodeoxygenation. (Reproduced from ref. 99 with permission from Elsevier. Copyright 2014.)

The conversion routes of anisole hydrodeoxygenation depends on the reaction conditions (e.g., temperature, H_2 pressure). Jin *et al.* found that Ni catalysts (activated carbon, SiO_2, SBA-15, and γ-Al_2O_3 as support) exhibited high activity for the saturation of aromatic ring at the relatively low temperature (180-210 ^oC) and moderate hydrogen pressure (0.5-3.0 MPa).[86] The selectivity to benzene *via* direct cleavage of C_{Ar}-O bond increased at lower H_2 pressure (*e.g.* atmospheric pressure, **Figure 8**).

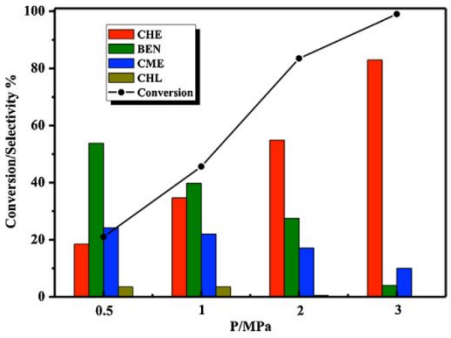

Figure 8. Pressure dependence of conversion and selectivity toward main products in HDO of anisole. Reaction condition: 8 wt% anisole (1.2 g, 0.0108 mol) dissolved in 20 mL n-decane, 0.1 g reduced catalysts (Ni/SiO_2), 210 ^oC, 700 rpm stirring speed. (Reproduced from ref. 86 with permission from Elsevier. Copyright 2014.)

Moreover, the dispersion of nickel species and the synergy between metallic sites and acid sites are key to the hydrogenation of anisole on supported nickel catalysts.[86,115] Anisole HDO over Ni supported on different supports (SBA-15, Al-SBA-15, γ-Al_2O_3, microporous carbon, TiO_2 and CeO_2) was conducted in a flow reactor at relatively low hydrogen pressure (0.3 Mpa) and moderate temperature (290–310 ^oC).[99] The low H_2 pressure, relatively high temperature and low space velocity favored the formation of aromatic products. In addition, the product distribution was regulated by the acidity and metal dispersion. Properties of supports influenced the dispersion of active phases. The weak acidity of C promoted the adsorption of Ni cations on the support. Besides, the incorporation of Ni generated additional acidity on the catalysts. Both weak and strong acidity sites were observed over Ni/C catalyst by NH_3-TPD. The yield of aromatic products could

be further increased to 65% (310 °C, 0.3 MPa, WHSV= 20.4 h^{-1}) over Ni/C catalyst due to the high dispersion of Ni and acidity of catalyst. Tu *et al.* fabricated Ni/IM-5 catalyst by hydrothermal synthesis.[116] The microporous and mesoporous channels of the support promoted the dispersion of Ni species and enhanced the interaction between NiO and the IM-5 zeolite. Both TEM and CO-FTIR results confirmed the high dispersion of Ni species on IM-5 support. The introduction of nickel species caused the formation of new medium-acid sites and increased the amount of weak acid compared with the support according to NH_3-TPD profiles. Compared to the catalyst prepared by hydrothermal method, both the acid amount and acid strength decreased on catalyst prepared by metal infiltration, possibly due to the blockage of acid sites in the micropores by Ni particles. The catalyst prepared by impregnation method showed more microporous area (233 m^2/g) than the sample synthesized by hydrothermal method (208 m^2/g), indicating that hydrothermal method could load Ni particles into the microporous channels more efficiently. The high activity and selectivity to cyclohexane was attributed to the high dispersion of nickel species and the synergy between metallic sites and acid sites on the catalyst prepared by hydrothermal method that promoted the hydrogenation–dehydration route.

Incorporation of other elements (*e.g.* Cu, Ga, Ce) to tune the properties of Ni species has also been employed for the hydrodeoxygenation of anisole.[45] Yang *et al.* studied the effect of Ce/Si molar ratio on the hydrodeoxygenation of anisole on Ni/Ce-SBA-15 at 270-290 °C and H_2 pressure of 0.7 MPa in a flow reactor.[109] Increasing Ce/Si ratio could slightly enlarge the pore diameters of SBA-15 and samples with Ce/Si ratio of 0.001–0.03 had higher specific surface area and total pore volume than bare support. Moreover, the Ni particle sizes gradually decreased (from 8 nm to 3 nm) as adding Ce species to SBA-15, indicating the increase in Ni dispersion. The catalyst with Ce/Si = 0.03 exhibited the highest turnover frequency (TOF) for HDO of anisole to benzene at 290 °C and it was ascribed to high dispersion of the metallic phase and the formation of specific active sites at the Ni^0-cerium oxide interface (**Table 4**). The introduction of Ga to Ni/SiO_2 generated Ni-Ga alloy and an intermetallic compound.[47] Ga not only diluted Ni ensembles into smaller ones (geometric effect), but also

transferred electron to Ni (electronic effect), which resulted in the enhancement in the hydrogenolysis route and suppression in both methanation and hydrogenation of aromatic ring.

Table 4. Anisole hydrodeoxygenation over 5% Ni/Ce-SBA-15 catalysts. (Reproduced from ref.109 with permission from Elsevier. Copyright 2016.)

Catalysts	Ce/Si molar ratio	Rate (μmol/s $g_{Cat.}$)		TOF[a] (s^{-1}) × 10^3	
		270 °C	290 °C	270 °C	290 °C
Ni/CeSi-001	0.001	0.22	0.50	1.3	5.8
Ni/CeSi-01	0.01	0.23	0.60	1.2	5.9
Ni/CeSi-03	0.03	0.54	0.97	2.4	7.9
Ni/CeSi-08	0.08	0.80	1.11	2.8	7.3

[a] For benzene production estimated from Ni dispersion.

Guaiacols (guaiacol, vanillin, *etc.*) are selected as model compounds because they contain both hydroxyl (−OH) and methoxy (−OCH_3) groups representative of lignin derived phenolic compounds. They therefore offer a useful compromise between analytical simplicity and model representativeness.[117] The strength of C–O bonds of guaiacol molecule follows the order: $C_{Ar}O$–CH_3(247 kJ/mol) < C_{Ar}–OCH_3(356 kJ/mol) < C_{Ar}–OH (414 kJ/mol).[118] Due to the presence of the aromatic ring and two oxygen-containing groups with three positions where the cleavage of C-O can happen, the reaction network of hydrodeoxygenation of guaiacol is very complicated. A typical one is shown in **Scheme 3**.

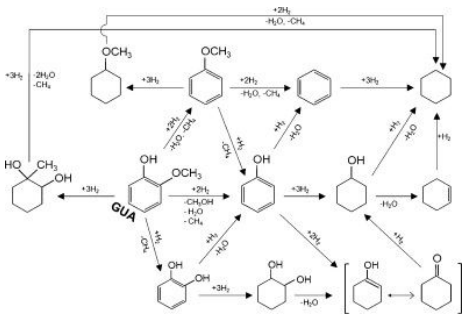

Scheme 3. Guaiacol conversion pathways over Ni-based catalysts. (Reproduced from ref. 55 with permission from Elsevier. Copyright 2012.)

Like the hydrodeoxygenation of phenol and anisole, low H_2 pressure and high reaction temperature can preserve the aromatic ring *via* direct hydrogenolysis route for guaiacol over nickel-based catalysts.[103,119] In contrast, high H_2 pressure and relatively low reaction temperature promote the saturation of aromatic ring as the first reaction step.

Supports with more surface acidity are beneficial for the HDO ability of the catalyst, but coke formation originating from the acidity is a disadvantage.[52,117,120,121,122] The formation rate of cyclohexane is positively correlated with the total number of acid sites (mainly Brønsted acid) on Ni/HBEA catalysts, implying that Brønsted acid sites are active for demethoxylation and dehydration reactions.[98] Ni/hierarchical ZSM-5 and Ni/microporous ZSM-5 with roughly the same dispersion of Ni were applied for the HDO of guaiacol.[123] Higher activity was achieved over catalysts with more acidity on the surface. Barton *et al.* confirmed the role of acid sites by comparing Ni/HZSM-5 with Ni/SiO_2 (inert support), finding that incomplete deoxygenation of guaiacol occurred over the latter because of the low activity for dehydration of cyclohexanol.[124] High selectivity to cyclic alcohol also is obtained over other Ni/support (ZrO_2, CeO_2, ZrO_2−CeO_2, MgO, Nb_2O_5 and carbon) catalysts.[51,71,87,125,126]

Metal-support interaction also influences the HDO of guaiacol. Zhang *et al.* observed that the strong interaction between Ni and the anatase TiO_2 caused the cross migration between TiO_2 and Ni species even at mild temperatures (300°C).[127] The migration of anatase TiO_2 onto Ni particles formed an amorphous TiO_2 overlayer and subsequently deactivated the Ni sites for activation of H_2 (**Figure 9**). However, the migration of Ni (< 1.5 wt %) onto anatase TiO_2 generated a new type of catalytic site that was highly dispersed and strongly interacted with the TiO_2 support. These sites were too small to be detected by high-resolution TEM (< 2 nm) and they were attributed to the high selectivity obtained in hydrodeoxygenation of guaiacol to phenol.

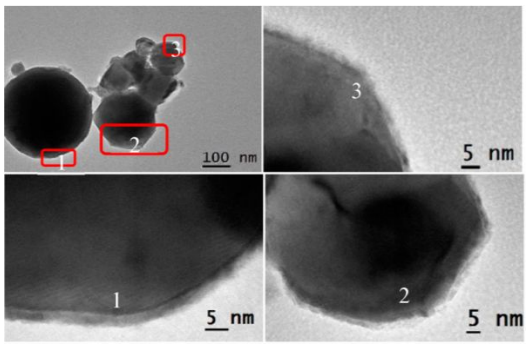

Figure 9. HRTEM images of SE-Ni 400/2 h. (Reproduced from ref. 127 with permission from American Chemical Society. Copyright 2019.)

A second metal (*e.g.* Fe, Mo, Cu, Co) is often incorporated onto nickel catalysts in the HDO of guaiacols.[40,128,129,130] The promotional effect of oxophilic metals (*e.g.* Fe, Mo) is interpreted as the facile activation of C-O bonds over the oxophilic sites.[79,131] Mo^{6+}, Mo^{5+}, Mo^{4+} and Mo^0 species co-existed on the reduced $NiMo/Al_2O_3–TiO_2$ catalysts.[54] The observation that higher reduction temperature could increase both the relative amount of Mo^0 (from 9% to 22%) and HDO activity (from 39% to 100%) led to the conclusion that Ni^0 and Mo^0 were active sites for guaiacol HDO. Guaiacol conversion of 98% and 100% selectivity to hydrocarbon (85% cyclohexane, 13% methylcyclohexane and 2% toluene) was achieved on $NiMo/Al_2O_3–TiO_2$ catalyst with 10 wt% Ni and 20 wt% Mo at 300 °C, 2 MPa in a flow reactor. The introduction of Co to nickel catalysts favors the formation of cyclic alcohol rather than hydrocarbons in the HDO of guaiacols.[53,132] The formation of NiCo alloy and oxygen vacancies on CoO_x was proposed to account for the high selectivity to alcohol. Positive roles of other species (*e.g.* Cu, Ga, La, Sm, Ce, W) have also been reported.[84,117,133,134]

Solvents are frequently used to dissolve reactants and they have a dramatic effect on guaiacol conversion and product distribution.[130] Some solvents (*e.g.* isopropanol) may decompose on the catalysts (*e.g.* $CoNi/Al_2O_3$) and provide H species to promote HDO reactions.[132] The solvent effect is complicated, and little research effort has been dedicated to this topic. Water was a better solvent than methanol and ethanol in the hydrodeoxygenation of guaiacol over $NiCo/\gamma\text{-}Al_2O_3$ catalysts (**Table 5**).[53] Possible reasons were that methanol would react with intermediates during guaiacol HDO or methanol/ethanol would competitively adsorb on the active sites. Solvent effects also depend

on the choice of catalysts for the hydrodeoxygenation reaction because of the difference in chemical and physical properties of solvents and catalysts. In the HDO of eugenol, a conversion of 96.2% and a selectivity to hydrocarbons of 44.3% were achieved over Ni.AC in water.[135] At the same reaction conditions, the conversion decreased to 67% and selectivity to hydrocarbons decreased to 7.4% over Ni/AC in n-hexane. In contrast, the conversion increased from 63.9% to 100% and selectivity to hydrocarbons increased from 70.7% to 90% over Ni/HZSM-5 when replacing water with n-hexane as solvent. The dramatically different performance profiles were ascribed to the discrepancies of catalyst dispersion and reactant solubility in different solvents.

Table 5. Effect of Solvent on Guaiacol Conversion and Product Distribution[a]. (Reproduced from ref. 53 with permission from American Chemical Society. Copyright 2017.)

			selectivity			
entry	catalysts	guaiacol con (%)	COL	COE	t-MCOL	c-MCOL
1	water	96.0	70.9	0.36	12.9	8.1
2	methanol	40.1	31.9	2.2	29.4	23.9
3	ethanol	48.1	32.6	1.1	32.8	22.4

[a] COL: cyclohexanol. COE: cyclohexane. t-MCOL: 1-methyl-1,2- cyclohexanediol, trans. c-MCOL: 1-methyl-1,2-cyclohexanediol, cis.

3.2 HDO of Furanic Compounds

Furan-derived compounds (*e.g.* furfural, hydroxymethylfurfural, benzofuran, *etc.*) are also found in bio-oils.[22,36,136,137] The -CHO group in furfural and hydroxymethylfurfural can cause instability in bio-oils. Moreover, the hydrodeoxygenation of hydroxymethylfurfural (HMF) to dimethylfurfural (DMF) has received much attention since Dumesic's group proposed the production of HMF by selective dehydration of fructose.[138] DMF is regarded as a promising liquid fuel because it has high boiling point, high energy density, and low solubility in water. A typical conversion route is shown in **Scheme 4**.[139]

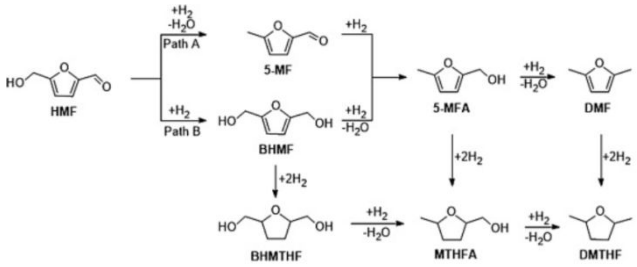

Scheme 4. Reaction pathway of HMF hydrodeoxygenation. (Reproduced from ref. 139 with permission from Elsevier. Copyright 2020.)

Hydrodeoxygenation of HMF over nickel catalysts is highly influenced by process parameters (*e.g.* reaction temperature, H_2 pressure). Typical temperature and pressure are 150 - 220 °C and 0.25 MPa - 5MPa. Too high temperature (*e.g.* 250 °C) causes ring hydrogenation, ring cracking, coke formation and other side reactions.[57,140,141] The conversion routes are proposed to depend on the adsorption mode of furan-derived compounds on the surface of catalysts.[142] That decarbonylation of HMF proceeds through η^1(C)-acyl species (**Scheme 5a**), resulting in the formation of furfuryl alcohol and CO.[143,144] 2,5-Bis(hydroxymethyl)furan (BHMF) is produced from hydrogenation of C=O bond *via* η^2(C, O)-aldehyde species (**Scheme 5b**) or η^1(O)-aldehyde species (**Scheme 5c**).[145,146] 5-methylfurfural (5-MF) could be formed *via* furoxy species (**Scheme 5d**) by abstracting hydrogen from -OH of HMF followed by C-O bond cleavage of the furoxy species.[142,145]

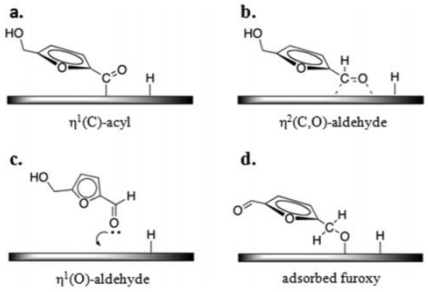

Scheme 5. Proposed oxygenate intermediates species for the conversion of HMF on transition metal surfaces. (Reproduced from ref. 142 with permission from American Chemical Society. Copyright 2016.)

Kinetic studies of HMF HDO have been performed to reveal the rate determining steps related to the C-O and C=O bonds. The hydrogenation of HMF to BHMF was the rate-determining step over Ni/C catalysts at 150-190°C, 10 Mpa.[147] Typical side reactions (the formation of 2,5-bis(hydroxymethyl)tetrahydrofuran (BHMTHF) and 2,5-dimethyltetrahydrofuran (DMTHF)) were kinetically blocked, which explained the high selectivity to DMF. Duarte *et al.* suggested that hydrogenation of the HMF carbonyl group was faster than

hydrogenolysis of the HMF hydroxyl group over Ni/γ-Al_2O_3 catalyst as 5-MF was absent even at low reaction temperatures.[142] Zhu *et al.* found that the reaction route of HMF HDO over CuNi/biochar catalyst was controlled by temperature.[141] At low temperature (around 100 °C), the HDO of HMF first underwent the hydrogenation of C=O group. When the temperature was high enough, the hydrogenolysis of -OH of HMF would be the first step (**Figure 10**).

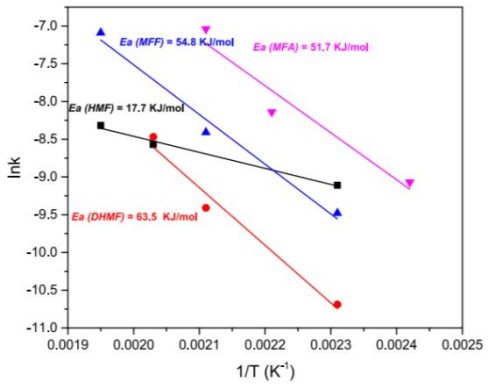

Figure 10. Profiles of Arrhenius plots of different intermediates in the HDO of HMF over 5% Cu−15% Ni/BC: black line HMF as substrate, red line DHMF as substrate, blue line MFF as substrate, and purple line MFA as substrate. Reaction conditions: $M_{substrate}$ = 1.98 × 10^{-3} mol, $m_{5\%Cu-15\%Ni/BC}$ = 100 mg, V_{THF} = 40 mL. (Reproduced from ref.141 with permission from American Chemical Society. Copyright 2019.)

Unlike the hydrodeoxygenation of aromatic oxygenates, in which the hydrogenation of aromatic ring is preferential, the furan ring is usually preserved in HDO of furanic compounds at low temperature (*e.g.* 200 °C). The -OH group in HMF, 2, 5-bishydroxymethylfuran (BHMF) and 5-methyl-furfurylalcohol (MFA) is removed by direct hydrogenolysis due to the presence of the furan ring. Thus, most of the attention on the design of nickel catalysts for HMF HDO focuses on the dispersion of metallic site, Lewis acidity and the interaction between metallic sites and support instead of the Brønsted acidity.[139,148,149]

Kong *et al.* prepared NiSi-phyllosilicate catalyst *via* ammonia evaporation method and then applied it to the HDO of HMF in a batch reactor.[61] Both highly dispersed Ni^0 sites and coordinatively unsaturated Ni^{2+} sites at nickel phyllosilicate were closely present on the reduced catalyst (**Figure 11**). Compared to impregnated catalyst with a similar loading amount of Ni, NiSi-phyllosilicate catalyst had much

smaller particle size and much higher/larger surface properties (*e.g.* specific surface area, pore volume, pore size, specific surface area of Ni and acid density). The catalyst showed much higher intrinsic activity (1404 h^{-1}) and hydrogenolysis rate (1487 h^{-1}) for HDO of HMF than impregnated Ni/SiO_2 catalyst (703 h^{-1} and 479 h^{-1}, respectively) at low temperature. Full conversion of HMF and 72.9% DMF selectivity were obtained at 130 °C, H_2 pressure of 1.5 Mpa, 0.15 g of NiSi-phyllosilicate catalyst, 1.5 g of HMF in 38 ml of 1,4-dioxane and 3h reaction time. The superior performance was attributed to the synergy between highly dispersed Ni^0 sites and coordinatively unsaturated Ni^{2+} sites in proximity. Ni^0 sites were proposed to dissociate H_2 and hydrogenate the C=O bond while coordinatively unsaturated Ni^{2+} sites activated the C−O bond. Similar effects were also observed over Ni/ZrP catalysts.[58] Siddiqui *et al.* studied the HDO of HMF over Ni/WO_3 at 100–200 °C in a batch reactor.[150] Full conversion of HMF and 95% DMF selectivity was achieved at pressure 180 °C and 1 MPa of H_2 over 6h of reaction, with DHMF and MFOL as the main intermediates. The enhanced activity was ascribed to the presence of highly dispersed Ni NPs on the WO_3.

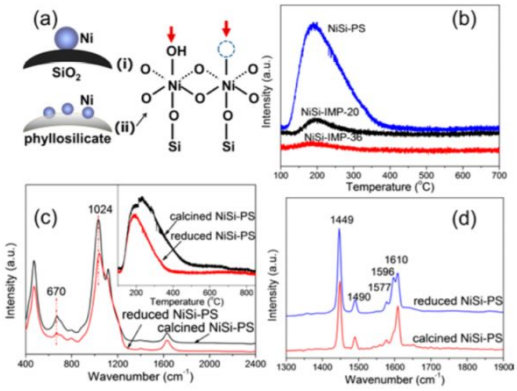

Figure 11. Characterizations of surface acidity. (a) Schematic representation of reduced impregnated Ni/SiO_2 catalysts, NiSi-PS and origin of surface acidity. (b) NH_3-TPD results of reduced catalysts, (c) FT-IR and NH_3-TPD results of calcined and reduced NiSi-PS catalysts, and (d) Py-IR spectra of calcined and reduced NiSi-PS catalysts. (Reproduced from ref. 61 with permission from American Chemical Society. Copyright 2015.)

Copper is often incorporated to nickel catalysts for HDO of furan-derived compounds.[151] The synergistic effect between Cu and Ni in terms of geometric effect and electronic effect has been observed by many researchers.[77,152] The HDO of HMF was facilitated by a synergistic effect between CuNi alloy and Lewis acid sites on NiO_x species over CuNi/biochar catalyst (**Scheme 6**).[141] The bimetallic

catalyst (5% Cu−15% Ni/BC) had a much higher TOF(DMF, 128.1 h^{-1}) than monometallic Ni catalyst (22.4 h^{-1}) although 15% Ni/BC had a higher dispersion of Ni (3.2% for monometallic catalyst and 1.9% for bimetallic catalyst). NiO_x species adsorbed and activated the C=O bond *via* the O atom. The electron transfer from Cu to Ni promoted the β-hydride elimination and C−O hydrogenolysis of HMF. Besides, a proper ratio of Lewis acid/metal active sites (2.49) significantly influenced the HDO of HMF to DMF. Tang *et al.* found that alloying Ni with Cu could downshift the *d*-band center of Ni.[153] It not only improved the catalytic activity by promoting the desorption of H species from Ni surface but also tailored selectivity by transforming the adsorption orientation of furfural.

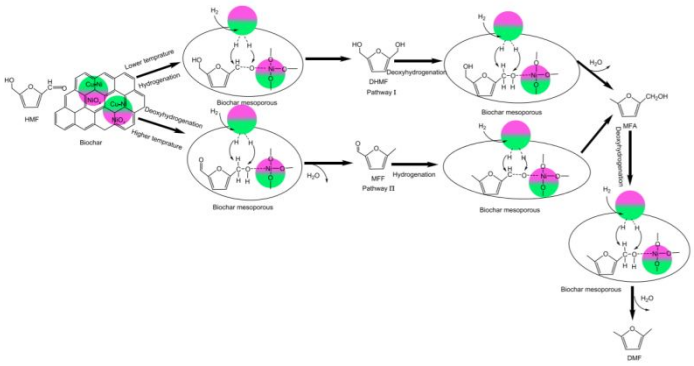

[a]The pink represents NiOx, and the green represents Cu−Ni alloy.

Scheme 6. Plausible Reaction Mechanism for the HDO of HMF to DMF over the Cu−Ni/BC Catalyst[a]. (Reproduced from ref.141 with permission from American Chemical Society. Copyright 2019.)

Supports have effects on the interaction between Ni and Cu and surface distribution of each metal, which subsequently influence the catalytic properties. Generally, Cu segregates on the NiCu bimetallic surface because Cu has a lower surface energy than Ni in vacuum. However, the introduction of support usually causes interaction between support and metals and provide additional changes in their surface distribution. The TiO_2 of $CuNi/TiO_2$ catalyst caused Ni species to be enriched at the TiO_2 interface. The formation of the Cu-shell and Ni-core structures contributed to the enhanced HDO activity and high selectivity to methylated furans (**Figure 12**).[154] When employing Al_2O_3 as support, Ni accumulated into continuous domains which had minimal interaction with Cu on the surface, leading to the hydrogenation of furan ring.[64] However, a $NiCu_3$ phase was found on NiCu/C catalyst consisting of a Cu-rich core and a 1:1 molar Ni: Cu shell.[62] Wang

et al. observed the formation of NiCu alloy on the $NiCu/Nb_2O_5$ catalyst.[155] The bimetallic catalyst exhibited more active sites for the activation of H_2 than Ni/Nb_2O_5, resulting in high catalytic activity of $NiCu/Nb_2O_5$ in the HDO of 4-(2-furanyl)-3-butene-2-one.

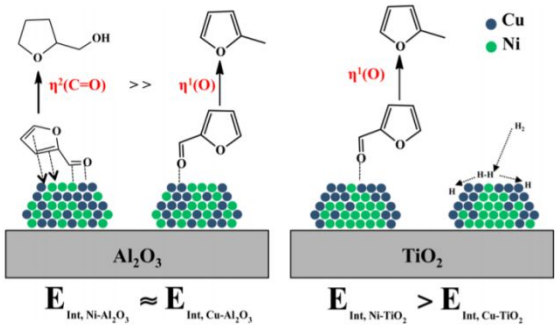

Figure 12. Schematic diagram of the proposed operating states of Cu−Ni bimetallic catalysts on Al_2O_3 and TiO_2. For $Cu−Ni/Al_2O_3$, significant exposure of extended Ni domains drives efficient ring hydrogenation to form THFOL, whereas the segregated structure of Cu−Ni on TiO_2 facilitates MF formation. E_{INT}: Energy of interaction between metal (either Ni or Cu) and support (Al_2O_3 and TiO_2). (Reproduced from ref.154 with permission from American Chemical Society. Copyright 2020.)

Other metals have also been found beneficial when added to nickel catalysts for the HDO of HMF. The introduction of Zn to Ni/Al_2O_3 catalyst generated β1-NiZn alloy species on the surface.[156] Ni atoms were not only geometrically isolated but also electron-enriched by Zn atoms, which led to a significant increase in the ratio of C-O hydrogenolysis rate over C-C cracking rate on $NiZn/Al_2O_3$ catalyst compared with Ni/Al_2O_3 (**Figure 13**). The oxyophilic Fe sites in NiFe alloy could stabilize the η^2-(C,O) adsorption of furfural and thus suppressed the undesired decarbonylation of furfural to furan and over-hydrogenation of furan ring over NiFe/C catalyst.[63,157,158]

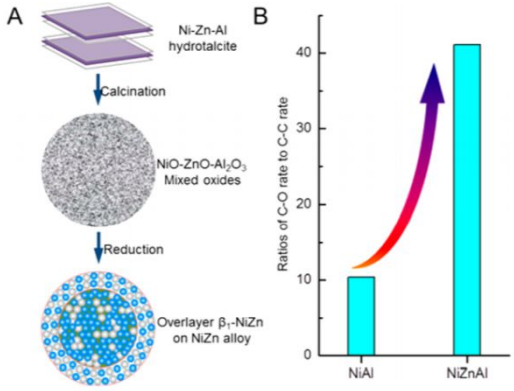

Figure 13. (A) Structure evolution of the NiZnAl catalyst and (B) comparisons of rate for C−O conversion to C−C conversion under similar conversions. (Reproduced from ref. 156 with permission from American Chemical Society. Copyright 2017.)

Typical solvents used in the hydrodeoxygenation of furan-derived compounds are THF, water, 1-propanol, 1,4-dioxane, *etc.* Common concerns regarding choosing a solvent involve the solubility of reactants and intermediates, the reactivity of solvent with substrates and the stability of solvent at the reaction condition. Gyngazova *et al.* studied effect of 7 solvents on the performance of HDO of HMF over Ni/C catalysts.[147] They found that the reaction with tetrahydrofuran (THF) and 2-methyl-THF as solvent could have high conversion of HMF, high selectivity to DMF and solvent stability. It was found that 2-methyl-THF was a better solvent than THF, because water was formed during the HDO and 2-methyl-THF had a lower water miscibility. Water was the best solvent among water, ethanol, isopropanol, THF and hexane for HDO of HMF over Ni/WO_3 (**Table 6**).[150] When hydrodeoxygenation of furfural was performed, isopropanol was a better H_2 donor and solvent than methanol to achieve high yield to 2-methylfuran due to a lower reduction potential of isopropanol.[159]

Table 6. Effect of different solvents on the HMF hydrogenation. (Reproduced from ref.150 with permission from the Royal Society of Chemistry. Copyright 2018.)

			Product selectivity (%)			
S. No.	Solvent	Con. (%)	BHMF	MFA	DMF	Others
1	Water	99	2.1	1.9	95	0
2	Ethanol	47	65	2.8	24.6	7.6
3	Isopropanol	49	64.6	1.4	29	3.6
4	THF	13	12.8	34.6	40.8	11.8
5	Hexane	9.8	48.7	1.3	17.7	32.3

3.3 HDO of Carboxylic Acids and Esters

A typical conversion route for hydrodeoxygenation of carboxylic acids and esters over nickel catalysts is shown in **Scheme 7**.[67] The dispersion of metallic sites, the properties of support (acid/base sites) and the synergy among different functionalities often govern the catalytic activity and product distributions at a given reaction condition.[82,160,161,162,163] Ni^0 sites favor H_2 dissociation, decarbonylation / decarboxylation, hydrogenolysis of C-O bond and hydrogenation reactions, while Brønsted acid sites catalyze the dehydration of alcohol.[162]

Cracking and isomerization of the carbon chain also occur depending on the type and strength of acid sites.[164,165,166] It is also found that lower H_2 pressures promote decarbonylation/decarboxylation while higher H_2 pressures facilitate the HDO route. Increasing reaction temperature could promote the conversion but too high temperature usually causes the cracking of alkanes.

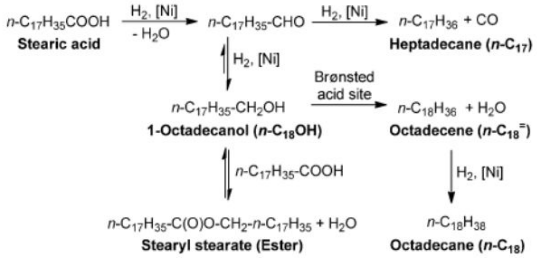

Scheme 7. Proposed reaction network for the hydrodeoxygenation of stearic acid, showing the decarbonylation route towards n-heptadecane (C17), dehydration/hydrogenation to n-octadecane (C18), and reversible esterification towards stearyl stearate. (Reproduced from ref. 67 with permission from Wiley-VCH Verlag GmbH & Co. KGaA, Weinheim. Copyright 2017.)

Alkanes with one less carbon atom are usually obtained in the deoxygenation of carboxylic acids and carboxylic acid esters over nickel catalysts, such as Ni/ZrO_2, *via* the decarbonylation/decarboxylation route.[160,161,167] Ni sites alone could hydrogenate stearic acid to aldehyde over Ni/ZrO_2 catalysts.[168] The oxygen vacancy of ZrO_2 could facilitate the adsorption of stearic acid *via* carboxylic group and generate carboxylate species, which was subsequently converted to a ketene intermediate by abstracting an α-hydrogen atom. Ni sites were then involved to transform ketene into aldehydes and then decarbonylate aldehydes to C17 alkane (**Figure 14**).

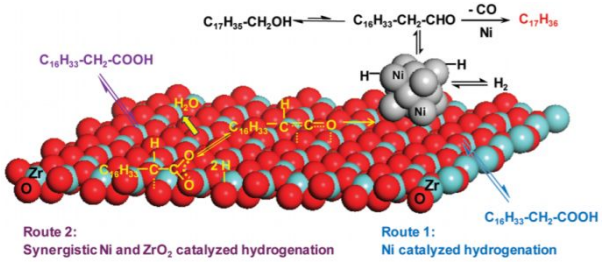

Figure 14. Proposed reaction mechanism for deoxygenation of stearic acid to C17 n-heptadecane via synergistic catalysis over Ni/ZrO_2. (Reproduced from ref.168 with permission from American Chemical Society. Copyright 2012.)

The hydrodeoxygenation route (hydrogenation-dehydration-hydrogenation) is preferred as it can preserve the carbon chains. Moreover, CO and CO_2 formed *via* decarbonylation/decarboxylation route could react with H_2 over Ni sites to produce CH_4 and H_2O (methanation), which increases the consumption of H_2. Different strategies have been proposed to facilitate the hydrodeoxygenation route. As the dehydration reaction is catalyzed mainly by Brønsted acid sites, introducing Brønsted acidity to the catalysts could improve the selectivity to products.[166,169] Foraita *et al.* studied the hydrodeoxygenation of stearic acid over Ni/SiO_2–ZrO_2 catalyst.[67] Unlike ZrO_2 which only had Lewis acid sites on the surface, the incorporation of SiO_2 to ZrO_2 created Brønsted acid sites and thus significantly promoted the hydrodeoxygenation route to produce 1-octadecene (**Figure 15**).

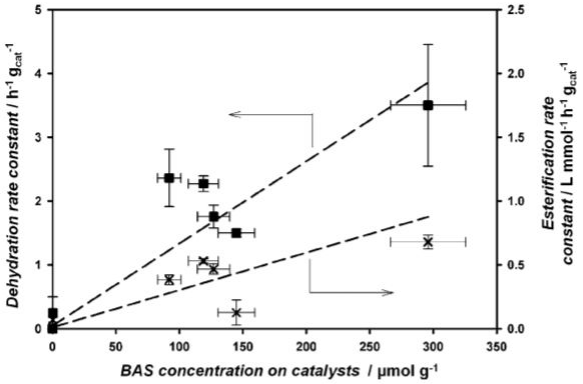

Figure 15. Rate constant for the dehydration of 1-octadecanol (square) and esterification of stearic acid and 1-octadecanol (cross) normalized to catalyst weight as a function of concentration of BAS on Ni/SiO_2–ZrO_2 catalyst. Reaction conditions: stearic acid (0.5 g), Ni/SiO_2–ZrO_2 catalyst (10 wt% Ni, 0.05 g), dodecane (100 mL), 260 °C, p(H_2)=40 bar, stirring at 600 rpm, 2 h. (Reproduced from ref. 67 with permission from Wiley-VCH Verlag GmbH & Co. KGaA, Weinheim. Copyright 2017.)

The use of zeolite (*e.g.* HY and HBEA) with suitable acid strength as support can improve the hydrodeoxygenation route over nickel catalysts, although the effect of acid strength on hydrodeoxygenation route is still controversial.[170,171] Ma *et al.* fabricated an interconnected hierarchical HUSY zeolite with high external surface area and obtained Ni/HUSY catalyst with high Ni loading (35 wt%) and high Ni dispersion (5.5%) *via* deposition-precipitation method.[172] Under a condition of 260 °C, 4 MPa of H_2, 80 mL dodecane, 0.2 g Ni/HUSY catalyst, 5.0 g stearic acid, and 600 rpm of stirring speed, Ni/HUSY-4 reached full conversion after 60 min with an initial rate of 60 g/(g·h). The main reaction route was the hydrogenation–dehydration–hydrogenation route, as evidenced by the high selectivity (96%) to C18

alkanes and attributed to high-strength Brønsted acid sites (**Scheme 8**). The high efficiency of the catalyst was ascribed to the synergy among the extra-framework AlOH group (Lewis acid), the bridging hydroxyl group (Brønsted acid), and highly dispersed Ni species. HBEA zeolite itself was found active in the hydrodeoxygenation of FAMEs under the condition of 270 °C, 1 MPa H_2, catalyst (0.1 g), FAMEs (1.0 g), dodecane (4.0 g), t=8 h, but exhibited very low activity (only 3.2% conversion).[13] Incorporating Ni onto HBEA not only preserved the hydrodeoxygenation route but also dramatically enhanced the catalytic activity. 100% conversion of FAMEs and 93.2 % of the selectivity to C15–C18 *via* hydrodeoxygenation route was achieved over 10 wt% Ni/HBEA(Si/Al=25) at 270 °C and H_2 pressure of 1.0 MPa after 8 h of reaction. Decarbonylation/decarboxylation was promoted only at high temperatures and low H_2 pressures over Ni/HBEA with higher Ni loadings.

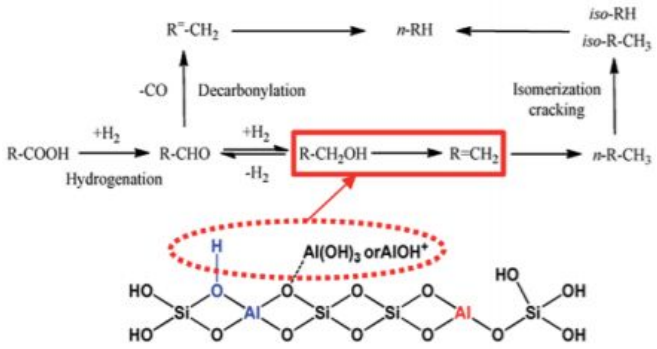

Scheme 8. Brønsted/Lewis acid synergy in HUSY zeolite promoted fatty alcohol dehydration. (Reproduced from ref.172 with permission from the Royal Society of Chemistry. Copyright 2016.)

Song *et al.* compared the effect of preparation methods (impregnation, ion exchange/precipitation, deposition–precipitation, and grafting as-synthesized Ni nanoparticles methods) on the performance of hydrodeoxygenation of stearic acid.[82] The loading amount of Ni on HBEA was kept at 5 wt % level. Samples prepared by impregnation and grafting as-synthesized Ni nanoparticles methods showed similar specific surface area and pore volume as the bare support, while other catalysts exhibited a decrease in specific surface area and pore volume. On the reduced samples, catalysts synthesized by impregnation had the largest particle size (25 nm) than others (2-4 nm). In the reaction, it

was observed that catalysts with small metal sites (samples prepared by deposition–precipitation) showed high initial rates (18 mmol*g^{-1}*h^{-1}) and catalysts with narrow range of particle sizes (samples prepared by deposition–precipitation and grafting as-synthesized Ni nanoparticles methods) exhibited high catalytic stability (4 runs).

Cu, Mo, Fe and Sn are frequently used to improve the performance of supported Ni catalysts in the deoxygenation of carboxylic acids and carboxylic acid ester.[173,174,175,176] Cu has geometrical and electronic effect on Ni, which promotes the reducibility of Ni and inhibits the cracking of the C-C bond.[177,178] Stearic acid was first hydrogenated to 1-octadecanal and then underwent decarbonylation to n-heptadecane over Ni_xCu_{1-x}/ZrO_2 catalyst. The incorporation of Cu generated Ni_xCu_{1-x} alloy species and Cu in the alloy increased the electron density of Ni, which then enhanced the binding strength of carbonyl group on Ni sites and promoted the subsequent decarbonylation (**Figure 16**).[68] Similar effects of Cu on Ni catalysts were also observed in the hydrodeoxygenation of methyl laurate over $NiCu/\gamma\text{-}Al_2O_3$.[179]

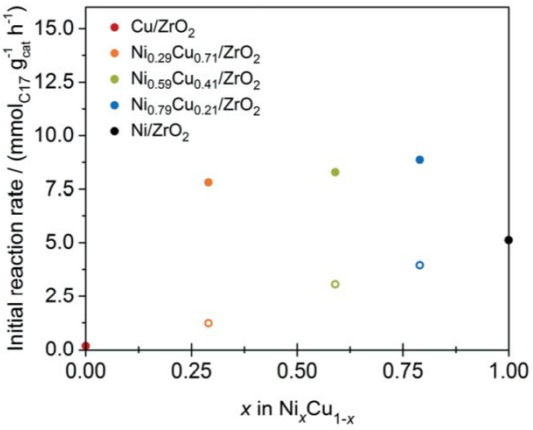

Figure 16. Decarbonylation reaction rate constant on Ni_xCu_{1-x}/ZrO_2 (x = 1, 0.79, 0.59, 0.29, 0) and physical mixtures of Ni/ZrO_2 and Cu/ZrO_2 (empty symbols) as a function of Ni content. Reaction conditions: stearic acid (0.5 g), Ni_xCu_{1-x}/ZrO_2 or x Ni/ZrO_2 1− xCu/ZrO_2 (x = 1, 0.79, 0.59, 0.29, 0; 0.2 g) n-dodecane (100 mL), 260 °C, p(H_2) = 4 MPa, 600 rpm. (Reproduced from ref.68 with permission from the Royal Society of Chemistry. Copyright 2019.)

Incorporating oxophilic metal (Fe, Mo, *etc*.) to nickel catalysts can significantly promote the hydrodeoxygenation route.[78,167,93,180] As Mo species have multiple valences and are very hard to be well reduced, the reduction temperature is a key governing factor in how Mo species interact with Ni. Mo^{6+} and Mo^{4+} species were found on the surface of $NiMo/Al_2O_3$ catalyst reduced at 400 °C for 2.5 h in H_2 and were

related to promote the HDO pathway in the hydrodeoxygenation of sunflower oil.[181] Chen *et al.* studied hydrodeoxygenation of methyl laurate over $NiMoO_{3-x}$/SAPO-11 reduced at different temperatures.[182] These samples exhibited similar specific surface area, pore volume and pore diameters. NH_3-TPD results showed the generation of new acid sites at 550 °C on samples reduced at 400, 450 or 500 °C apart from original acid sites at 260 °C and 350 °C. Loading NiMo species onto the support significantly increased the number of acid sites, but increasing the reduction temperature could gradually decrease the amount of acid sites. This led to the highest isomerization selectivity over catalyst reduced at 400 °C due to the highest acid concentration induced by Mo^{5+} sites. The particle sizes and dispersion of metal species were not significantly influenced by reduction temperature in terms of TEM and NO chemisorption results. NiO could be easily reduced to metallic Ni species while Mo species with different valences (Mo^{6+}, Mo^{5+} and Mo^{4+}) existed after reduction at 400-550 °C. Higher reduction temperature (from 450 to 550 °C) increased the amount of Mo^{4+} species (from 37.5% to 51.4%), which adsorbed C=O bond and -OH bond and thus accounted for the high selectivity to C12 alkanes *via* hydrodeoxygenation routes (**Scheme 9**).

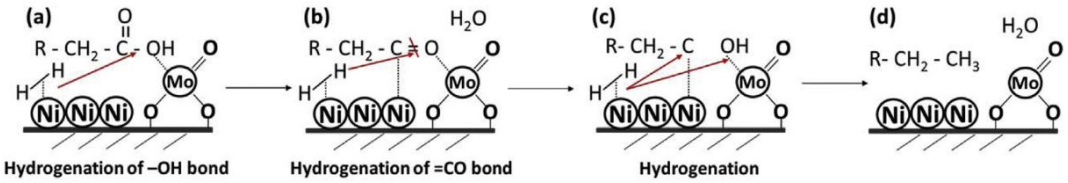

Scheme 9. Surface reaction model of CO hydrogenation for the hydrodeoxygenation of methyl laurate over the 450(500/550)R–NiMo catalyst (450, 500, 550: reduction temperature, °C, R: reduction). (Reproduced from ref. 182 with permission from Elsevier. Copyright 2015.)

3.4 HDO of Oxygenates Mixture

As the feedstocks for hydrodeoxygenation, especially bio-oils, contain hundreds of oxygenates, the intermolecular reactivity and mutual influence (*e.g.* competitive adsorption) in the hydrodeoxygenation over nickel catalysts are necessary knowledge for the design of HDO processes.[130,183] Zhang *et al.* compared the hydrodeoxygenation of individual model compounds (phenol, anisole, guaiacol, eugenol, cresol and vanillin) and their mixtures over Ni/SiO_2 and Ni/Al_2O_3 catalyst.[184] The results obtained over Ni/SiO_2 catalysts for hydrodeoxygenation of single phenolic compound and mixtures were similar. However, hydrodeoxygenation of mixtures produced significantly less hydrocarbons over Ni/Al_2O_3 compared with the yield of hydrocarbons obtained in the hydrodeoxygenation of single phenolic compound

over the same catalyst. This was explained by the adsorption of guaiacols (guaiacol, eugenol, and vanillin) on the mixture on the Lewis acidic sites on Ni/γ-Al_2O_3, which produced catechol and its derivatives as intermediates. These were then polymerized to the precursor of coke. As guaiacols and carboxylic acids were present in bio-oils, the hydrodeoxygenation of guaiacol and propionic acid mixture was studied over Ni/hierarchical ZSM-5, Ni/ SBA-15 and Ni/Al-SBA-15 catalysts.[185] The presence of propionic acid decreased the conversion of guaiacol to different extent depending on the support of catalysts. Propionic acid could form esters with alcohols, such as methanol from demethoxylation of guaiacol. Ni/hierarchical-ZSM-5 catalyst exhibited the highest HDO activity, possibly due to the highest acidity of the support.

3.5 HDO of Raw Feedstocks

Nickel and nickel-based bimetallic catalysts are also tested in the hydrodeoxygenation of raw feedstocks (*e.g.* bio-oils, waste cooking oil, algae oil).[186,187,188] Guo *et al.* studied the hydrodeoxygenation of algae oil on Ni−Cu/ZrO_2 catalysts. A maximum HDO efficiency of 82% with the yield to liquid product of 90% was reached on a Ni−Cu/ZrO_2 catalyst under the condition of 350 °C, H_2 pressure of 2 MPa; LHSV of 3.5 h^{-1}, H_2/oil (volume ratio) of 450 N m^3/m^3. Both the HDO efficiency and stability of the Ni−Cu/ZrO_2 catalyst surpassed the results obtained on NiMoS/Al_2O_3 catalyst.[189] Loe *et al.* applied 20% Ni/Al_2O_3 and 20% Ni–5% Cu/Al_2O_3 catalysts for the deoxygenation of algal lipids in a flow reactor. The content of diesel range hydrocarbons increased from ~7% to 78% over Ni/Al_2O_3 and 83% over NiCu/Al_2O_3 at time-on-stream (TOS) = 1 h.[176] However, the content of diesel range hydrocarbons decreased to 42% on Ni/Al_2O_3 and 45% on NiCu/Al_2O_3 at TOS = 4 h. As the feedstock contained a high amount of unsaturated fatty acid and compounds like phytols, these compounds could strongly adsorb on the active sites. Moreover, the unsaturated fatty acid could easily form coke on the active sites. The results highlight the importance of feedstock pretreatment and design of more robust catalysts. Hydrodeoxygenation of waste cooking oil was investigated over Ni/mesoporous HY catalyst with a C8–C16 yield of 40.5% and jet range aromatic hydrocarbons yield of 11.3% obtained at 400°C. The main conversion route is decarbonylation followed by cracking of long chain alkanes into C8–C16 hydrocarbons.[190]

One problem of bio-oil hydrodeoxygenation over Ni-based catalysts is the high yield of gas products, which originates from the types of feedstocks, the choice of catalysts and reaction conditions.[191,192,193,194,195] Jahromi *et al.* studied the hydrodeoxygenation of pinyon-juniper (PJ) catalytic pyrolysis oil using Ni/red mud catalysts in a batch reactor.[192] Organic liquid yield of 68.6% and gas (CH_4, CO, CO_2 and C_2H_4, *etc.*) yield of 16.4% were obtained using 40%Ni/red mud (RM) under the condition of 400 ^oC and H_2 pressure of 6.2 MPa. The oxygen content of pyrolysis oil decreased from 24.88 wt.% to 1.35 wt.% and heating value increased from 28.41 MJ/kg to 45.77 MJ/kg. Zhao *et al.* studied the hydrodeoxygenation of n-hexane-extracted crude pyrolysis oil over 20wt% Ni/HZSM-5(Si/Al = 45) catalyst.[196] The bio-oil was almost quantitatively converted to 15% of pentanes, 85% of C6–C9 cyclohexanes and trace amount of CO_2 in a semi-batch reactor at 250 ^oC, H_2 pressure of 5 MPa and stirring speed of 680 rpm for 4h reaction.

Coke formation is one of the major problems in the hydrodeoxygenation of raw feedstocks over supported Ni catalysts.[191,195,197,198,199] It originates from the Brønsted acidity of the catalysts, which is introduced to facilitate the dehydration step. Li *et al.* found that the types of coke formed on the Ni/HZSM-5 catalyst in the HDO of bio-oil depended on reaction temperature.[197] Polyaromatics were produced by aromatization, dehydrogenation, and hydrogen transfer reactions at higher temperatures (>280 °C) and coke of aliphatic compounds were formed by aromatization and rearrangement reactions at lower temperatures. The coupling of oxygenates and protons on Brønsted acid sites of HZSM-5 produced carbocations, which were precursors of graphite carbon. The incorporation of Cu to catalysts could significantly decrease the amount of coke formed on the catalyst (*e.g.* 19% to 9%), although the detailed mechanisms are not clear yet.[176,198]

Trace elements from bio-oil (*e.g.* sulfur, chlorine, phosphorus and alkali metals) can also cause the deactivation of Ni-based catalysts in the long-term hydrodeoxygenation reaction.[200,201] Unlike coke that can be removed by regeneration, the inorganic species are persistent on the surface. However, relevant research is scarce in literature. As sulfur could react with Ni to form stable nickel sulfide, it deactivated the catalysts quickly (12 h).[202] The amount of sulfur which could completely deactivate Ni/ZrO_2 was roughly equivalent to the amount of

available Ni (1.1 mol_S/mol_{Ni}). Similarly, Ni_3S_2 was detected on the surface of sulfur-deactivated $NiCu/Al_2O_3$ catalyst.[201] A steady decrease in catalytic activity of Ni/ZrO_2 was observed when introducing 0.05 wt% Cl into reactor over 40 h and the extent was similar to sulfur-induced one. However, the catalytic activity could be resumed when the feeding of Cl was stopped, indicating that the Cl-induced deactivation was not permeant. K^+ did not significantly influence the hydrogenation activity of Ni/ZrO_2, but markedly decreased its deoxygenation activity (from 90% to 20%), which was attributed the blocking of low-coordination sites by K^+. However, it was also proposed that K, Mg, Ca species mainly deposited on the support.[201]

4. Summary and Perspectives

The hydrodeoxygenation of biomass derived oxygenates to fuels is a potential way to alleviate the dependence on fossil fuels. Comprehensive design of the process, including the production and pretreatment of feedstocks (*e.g.* bio-oils and bio-diesels), hydrodeoxygenation reactions, and improved reactors, is required to improve the process efficiency. The development of HDO catalysts is one of the most important and difficult challenges due to the complexity in the compositions of feedstocks, the presence of large amount of water and process characteristics. Nickel has exceptional ability for H_2 decomposition, but it is also very active for many undesired reactions (*e.g.* cracking, methanation) in hydrodeoxygenation. Thus, tailoring the properties of nickel is the core topic in the design of nickel based HDO catalysts. Introducing different functionalities can improve the performance of nickel catalysts in the hydrodeoxygenation reactions, but there are still many problems in practice, such as sintering, and coke induced deactivation and high yield of gas products.

To cope with these difficulties, materials (supports and active species) discovery and more strategies about combining different functionalities should be highlighted. Compared with the extensive research activities on HDO reactions, much less efforts are spent on the innovations in catalyst synthesis. The common method for the preparation of nickel and nickel based bimetallic catalysts is

652 impregnation with traditional support (*e.g.* SiO_2, Al_2O_3). It is the simplest method, but it suffers from problems such as the low dispersion
653 of active species. Catalysts prepared by other methods, such as deposition-precipitation and ion-exchange method, have higher dispersion
654 of active species and usually exhibit higher catalytic activity in HDO reactions. Moreover, the distribution of active species and extent of
655 interactions among active species and supports are influenced by catalyst preparation method. Excellent supports usually introduce
656 necessary functionalities into the catalytic systems to achieve a synergistic effect. The use of supports with more Brønsted acidity has been
657 demonstrated to be beneficial to HDO reaction compared with inert supports.
658
659 More mechanistic insights into the HDO reactions and structural evolution of nickel and nickel based bimetallic catalysts in reactions are
660 necessary to facilitate the target reactions and suppress the side reactions. Good HDO catalysts usually achieve the synergy between
661 metallic sites and acid sites and a suitable interaction between Ni and the other metal species. However, the detailed mechanisms of the
662 synergy and interactions that determine the catalytic activity and selectivity have not been sufficiently elucidated. Moreover, understanding
663 the adsorption modes of oxygenates on the catalysts is critical to understand the mechanisms. Thus, *in situ* characterization of catalysts
664 and *operando* experiments are recommended for future research. In addition, detailed kinetics studies on individual steps can provide a
665 much clearer picture about reactions as HDO involves many parallel and sequential reactions.
666
667 Coke formation and sintering usually account for the deactivation of nickel and nickel-based bimetallic catalysts, but the mechanisms are
668 not well understood yet. One of the advantages of bimetallic catalysts over nickel catalysts, is that bimetallic catalysts are more resistant
669 to coke formation and sintering. Elucidation of the inherent mechanisms could help design catalysts with improved stability, and preventing
670 catalyst deactivation should considered at the early stage of catalyst design and preparation. More studies on deactivation of catalysts
671 induced by other poisons (*e.g.* S, Cl, P) are also necessary for the development of Ni-based HDO catalysts with good stability.
672

Using individual model compounds for HDO can allow necessary information about the catalysts and reactions to be obtained. However, considering the complex compositions of feedstocks (*e.g.* bio-oil and bio-diesel), the mutual influence among different oxygenates in HDO reactions cannot be neglected. Thus, more investigations using two or more oxygenates or raw feedstocks as substrate are critical to advance the development of new Ni-based catalysts that will have practical application for HDO.

Acknowledgement

This work was supported by National Science Foundation of United States (# CBET-1510157) and National Science Foundation of United States - Industry/University Cooperative Research Center for Rational Catalyst Synthesis (# IIP-1464630).

Reference

1. S. Z. Naji, C. T. Tye and A. A. Abd, *Process Biochemistry*, 2021, **109**, 148-168.
2. R. A. Sheldon, *Green Chemistry*, 2014, **16**, 950-963.
3. D. M. Alonso, J. Q. Bond and J. A. Dumesic, *Green Chemistry*, 2010, **12**, 1493-1513.
4. T. Kan, V. Strezov and T. J. Evans, *Renewable and Sustainable Energy Reviews*, 2016, **57**, 1126-1140.
5. A. Demirbas and G. Arin, *Energy Sources*, 2002, **24**, 471-482.
6. W. N. R. W. Isahak, M. W. Hisham, M. A. Yarmo and T.Y. Y. Hin, *Renewable and Sustainable Energy Reviews*, 2012, **16**, 5910-5923.
7. P. C. Badger and P. Fransham, *Biomass and Bioenergy*, 2006, **30**, 321-325.
8. K. Raffelt, E. Henrich, A. Koegel, R. Stahl, J. Steinhardt and F. Weirich, In Twenty-Seventh Symposium on Biotechnology for Fuels and Chemicals; McMillan J. D., Adney W. S., Mielenz J. R., Klasson K. T., Eds.; Humana Press: Totowa, United States, 2006, pp 153.
9. D. Mohan, C. U. Pittman Jr and P. H. Steele, *Energy & Fuels*, 2006, **20**, 848-889.
10. M. Saidi, F. Samimi, D. Karimipourfard, T. Nimmanwudipong, B. C. Gates and M. R. Rahimpour, *Energy & Environmental Science*, 2014, **7**, 103-129.
11. D. Y. Leung, X. Wu and M. Leung, *Applied Energy*, 2010, **87**, 1083-1095.
12. F. Ma and M. A. Hanna, *Bioresource Technology*, 1999, **70**, 1-15.
13. L. Chen, J. Fu, L. Yang, Z. Chen, Z. Yuan and P. Lv, *ChemCatChem*, 2014, **6**, 3482-3492.
14. G. Li, F. Zhang, L. Chen, C. Zhang, H. Huang and X. Li, *ChemCatChem*, 2015, **7**, 2646-2653.
15. J. Wu, J. Shi, J. Fu, J. A. Leidl, Z. Hou and X. Lu, *Scientific Reports*, 2016, **6**, 1-8.
16. L. Chen, H. Li, J. Fu, C. Miao, P. Lv and Z. Yuan, *Catalysis Today*, 2016, **259**, 266-276.
17. G. Li, L. Chen, R. Fan, D. Liu, S. Chen, X. Li and K. H. Chung, *Catalysis Science & Technology*, 2019, **9**, 213-222.
18. D. Valencia, C. Zenteno, P. Morales-Gil, L. Díaz-García, D. Gómora-Herrera, E. Palacios-González and J.

Aburto, *New Journal of Chemistry*, 2020, **44**, 2435-2441.
19. A. Srifa, N. Viriya-empikul, S. Assabumrungrat and K. Faungnawakij, *Catalysis Science & Technology*, 2015, **5**, 3693-3705.
20. S. Chen, G. Zhou, H. Xie, Z. Jiao and X. Zhang, *Applied Catalysis A: General*, 2019, **569**, 35-44.
21. P. Kumar, S. R. Yenumala, S. K. Maity and D. Shee, *Applied Catalysis A: General*, 2014, **471**, 28-38.
22. G. W. Huber, S. Iborra and A. Corma, *Chemical Reviews*, 2006, **106**, 4044-4098.
23. S. Czernik and A. Bridgwater, *Energy & Fuels*, 2004, **18**, 590-598.
24. J. Lehto, A. Oasmaa, Y. Solantausta, M. Kytö and D. Chiaramonti, *Applied Energy*, 2014, **116**, 178-190.
25. N. Yan, Y. Yuan, R. Dykeman, Y. Kou and P. J. Dyson, *Angewandte Chemie International Edition*, 2010, **122**, 5681-5685.
26. H. Ohta, H. Kobayashi, K. Hara and A. Fukuoka, *Chemical Communications*, 2011, **47**, 12209-12211.
27. X. Zhu, L. L. Lobban, R. G. Mallinson and D. E. Resasco, *Journal of Catalysis*, 2011, **281**, 21-29.
28. C. R. Lee, J. S. Yoon, Y. W. Suh, J. W. Choi, J. M. Ha, D. J. Suh and Y. K. Park, *Catalysis Communications*, 2012, **17**, 54-58.
29. P. Lee and J. Schwarz, *Journal of Catalysis*, 1982, **73**, 272-287.
30. C. Bartholomew and R. Pannell, *Journal of Catalysis*, 1980, **65**, 390-401.
31. A. Renouprez, P. Fouilloux, G. Coudurier, D. Tocchetti and R. Stockmeyer, *Journal of the Chemical Society, Faraday Transactions 1: Physical Chemistry in Condensed Phases*, 1977, **73**, 1-10.
32. A. M. Robinson, J. E. Hensley and J. W. Medlin, *ACS catalysis*, 2016, **6**, 5026-5043.
33. E. Furimsky, *Applied Catalysis A: General*, 2000, **199**, 147-190.
34. D. C. Elliott, *Energy & Fuels*, 2007, **21**, 1792-1815.
35. H. Wang, J. Male and Y. Wang, *ACS Catalysis*, 2013, **3**, 1047-1070.
36. S. Kim, E. E. Kwon, Y. T. Kim, S. Jung, H. J. Kim, G. W. Huber and J. Lee, *Green Chemistry*, 2019, **21**, 3715-3743.
37. Y. Shi, E. Xing, J. Zhang, Y. Xie, H. Zhao, Y. Sheng and H. Cao, *ACS Sustainable Chemistry & Engineering*, 2019, **7**, 9464-9473.
38. F. Yang, D. Liu, Y. Zhao, H. Wang, J. Han, Q. Ge and X. Zhu, *ACS catalysis*, 2018, **8**, 1672-1682.
39. E. Kordouli, B. Pawelec, C. Kordulis, A. Lycourghiotis and J. Fierro, *Applied Catalysis B: Environmental*, 2018, **238**, 147-160.
40. T. He, X. Liu, Y. Ge, D. Han, J. Li, Z. Wang and J. Wu, *Catalysis Communications*, 2017, **102**, 127-130.
41. P.-J. Hsu, J.-W. Jiang and Y.-C. Lin, *ACS Sustainable Chemistry & Engineering*, 2018, **6**, 660-667.
42. W. Li, F. Li, H. Wang, M. Liao, P. Li, J. Zheng, C. Tu and R. Li, *Molecular Catalysis*, 2020, **480**, 110642.
43. X. Zhang, X. Chen, S. Jin, Z. Peng and C. Liang, *ChemistrySelect*, 2016, **1**, 577-584.
44. J. E. Peters, J. R. Carpenter and D. C. Dayton, *Energy & Fuels*, 2015, **29**, 909-916.
45. S. A. Khromova, A. A. Smirnov, O. A. Bulavchenko, A. A. Saraev, V. V. Kaichev, S. I. Reshetnikov and V. A. Yakovlev, *Applied Catalysis A: General*, 2014, **470**, 261-270.
46. T. L. Hewer, A. G. Souza, K. T. Roseno, P. F. Moreira, R. Bonfim, R. M. Alves and M. Schmal, *Renewable Energy*, 2018, **119**, 615-624.
47. Y. Zheng, N. Zhao and J. Chen, *Applied Catalysis B: Environmental*, 2019, **250**, 280-291.
48. X. Li, J. Zhang, B. Liu, J. Liu, C. Wang and G. Chen, *Fuel*, 2019, **243**, 314-321.
49. R. Fan, Z. Hu, C. Chen, X. Zhu, H. Zhang, Y. Zhang, H. Zhao and G. Wang, *Chemical Communications*,

2020, **56**, 6696-6699.
50. H. Jahromi and F. A. Agblevor, *Applied Catalysis A: General*, 2018, **558**, 109-121.
51. X. Wang, S. Zhu, S. Wang, J. Wang, W. Fan and Y. Lv, *Applied Catalysis A: General*, 2018, **568**, 231-241.
52. P. Yan, J. Mensah, A. Adesina, E. Kennedy and M. Stockenhuber, *Applied Catalysis B: Environmental*, 2020, **267**, 118690.
53. M. Zhou, J. Ye, P. Liu, J. Xu and J. Jiang, *ACS Sustainable Chemistry & Engineering*, 2017, **5**, 8824-8835.
54. D.-P. Phan, T. K. Vo, J. Kim and E. Y. Lee, *Journal of Industrial and Engineering Chemistry*, 2020, **83**, 351-358.
55. M. Bykova, D. Y. Ermakov, V. Kaichev, O. Bulavchenko, A. Saraev, M. Y. Lebedev and V. Yakovlev, *Applied Catalysis B: Environmental*, 2012, **113**, 296-307.
56. D. Mukherjee, R. Singuru, P. Venkataswamy, D. Damma and B. M. Reddy, *ACS Omega*, 2019, **4**, 4770-4778.
57. D. Guo, X. Liu, F. Cheng, W. Zhao, S. Wen, Y. Xiang, Q. Xu, N. Yu and D. Yin, *Fuel*, 2020, **274**, 117853.
58. C. Zhu, Q. Liu, D. Li, H. Wang, C. Zhang, C. Cui, L. Chen, C. Cai and L. Ma, *ACS Omega*, 2018, **3**, 7407-7417.
59. G. Li, N. Li, J. Yang, L. Li, A. Wang, X. Wang, Y. Cong and T. Zhang, *Green Chemistry*, 2014, **16**, 594-599.
60. P. Yang, Q. Cui, Y. Zu, X. Liu, G. Lu and Y. Wang, *Catalysis Communications*, 2015, **66**, 55-59.
61. X. Kong, Y. Zhu, H. Zheng, X. Li, Y. Zhu and Y.-W. Li, *ACS Catalysis*, 2015, **5**, 5914-5920.
62. J. Luo, M. Monai, C. Wang, J. D. Lee, T. Duchoň, F. Dvořák, V. Matolín, C. B. Murray, P. Fornasiero and R. J. Gorte, *Catalysis Science & Technology*, 2017, **7**, 1735-1743.
63. C. Wang, J. Luo, V. Liao, J. D. Lee, T. M. Onn, C. B. Murray and R. J. Gorte, *Catalysis Today*, 2018, **302**, 73-79.
64. B. Seemala, C. M. Cai, R. Kumar, C. E. Wyman and P. Christopher, *ACS Sustainable Chemistry & Engineering*, 2018, **6**, 2152-2161.
65. P. Yang, Q. Xia, X. Liu and Y. Wang, *Journal of Energy Chemistry*, 2016, **25**, 1015-1020.
66. F. Feng, Z. Shang, L. Wang, X. Zhang, X. Liang and Q. Wang, *Catalysis Communications*, 2020, **134**, 105842.
67. S. Foraita, Y. Liu, G. L. Haller, E. Baráth, C. Zhao and J. A. Lercher, *ChemCatChem*, 2017, **9**, 195-203.
68. C. Denk, S. Foraita, L. Kovarik, K. Stoerzinger, Y. Liu, E. Baráth and J. A. Lercher, *Catalysis Science & Technology*, 2019, **9**, 2620-2629.
69. J. C. Vedrine, *Applied Catalysis A: General*, 2014, **474**, 40-50.
70. G. Somorjai, in *Advances in Catalysis*, Elsevier, 1977, vol. 26, pp. 1-68.
71. A. Dongil, B. Bachiller-Baeza, I. Rodríguez-Ramos, J. Fierro and N. Escalona, *RSC Advances*, 2016, **6**, 26658-26667.
72. T. Chen, O. Kwon, R. Huang, C. Lin and J. M. Vohs, *Journal of Catalysis*, 2021, **400**, 294-300.
73. C. W. Lee, P. Y. Lin, B. H. Chen, R. G. Kukushkin and V. A. Yakovlev, *Catalysis Today*, 2021, **379**, 124-131.
74. J. Chen, Y. Zhu, W. Li, F. Luo, S. Li, X. Li, Y. Huang, A. Zhang, Z. Xiao and D. Wang, *Biomass and Bioenergy*, 2021, **149**, 106081.
75. M. Boudart and G. Djéga-Mariadassou, in *Kinetics of Heterogeneous Catalytic Reactions*, Princeton

University Press, 2014.
76. B. Gates, *Chemical Reviews*, 1995, **95**, 511-522.
77. J. Wu, G. Gao, J. Li, P. Sun, X. Long and F. Li, *Applied Catalysis B: Environmental*, 2017, **203**, 227-236.
78. H. Imai, M. Abe, K. Terasaka, T. Suzuki, X. Li and T. Yokoi, *Fuel Processing Technology*, 2018, **180**, 166-172.
79. H. Fang, J. Zheng, X. Luo, J. Du, A. Roldan, S. Leoni and Y. Yuan, *Applied Catalysis A: General*, 2017, **529**, 20-31.
80. P. M. Mortensen, J. D. Grunwaldt, P. A. Jensen and A. D. Jensen, *Catalysis Today*, 2016, **259**, 277-284.
81. E. J. Shin and M. A. Keane, *Industrial & Engineering Chemistry Research*, 2000, **39**, 883-892.
82. W. Song, C. Zhao and J. A. Lercher, *Chemistry–A European Journal*, 2013, **19**, 9833-9842.
83. X. Li, L. Chen, G. Chen, J. Zhang and J. Liu, *Renewable Energy*, 2020, **149**, 609-616.
84. M. M. Ambursa, P. Sudarsanam, L. H. Voon, S. B. Abd Hamid and S. K. Bhargava, *Fuel Processing Technology*, 2017, **162**, 87-97.
85. D. P. Gamliel, B. P. Baillie, E. Augustine, J. Hall, G. M. Bollas and J. A. Valla, *Microporous and Mesoporous Materials*, 2018, **261**, 18-28.
86. S. Jin, Z. Xiao, C. Li, X. Chen, L. Wang, J. Xing, W. Li and C. Liang, *Catalysis Today*, 2014, **234**, 125-132.
87. M. Lu, Y. Jiang, Y. Sun, P. Zhang, J. Zhu, M. Li, Y. Shan, J. Shen and C. Song, *Energy & Fuels*, 2020, **34**, 4685-4692.
88. R. Nie, H. Yang, H. Zhang, X. Yu, X. Lu, D. Zhou and Q. Xia, *Green Chemistry*, 2017, **19**, 3126-3134.
89. Q. Han, M. U. Rehman, J. Wang, A. Rykov, O. Y. Gutiérrez, Y. Zhao, S. Wang, X. Ma and J. A. Lercher, *Applied Catalysis B: Environmental*, 2019, **253**, 348-358.
90. T. M. Huynh, U. Armbruster, M. M. Pohl, M. Schneider, J. Radnik, D. L. Hoang, B. M. Q. Phan, D. A. Nguyen and A. Martin, *ChemCatChem*, 2014, **6**, 1940-1951.
91. F. Yang, N. J. Libretto, M. R. Komarneni, W. Zhou, J. T. Miller, X. Zhu and D. E. Resasco, *ACS Catalysis*, 2019, **9**, 7791-7800.
92. S. Xing, Y. Liu, X. Liu, M. Li, J. Fu, P. Liu, P. Lv and Z. Wang, *Applied Catalysis B: Environmental*, 2020, **269**, 118718.
93. X. Yu, J. Chen and T. Ren, *RSC Advances*, 2014, **4**, 46427-46436.
94. X. Yue, L. Zhang, L. Sun, S. Gao, W. Gao, X. Cheng, N. Shang, Y. Gao and C. Wang, *Applied Catalysis B: Environmental*, 2021, **293**, 120243.
95. Q. Chen, C. Cai, X. Zhang, Q. Zhang, L. Chen, Y. Li, C. Wang and L. Ma, *ACS Sustainable Chemistry & Engineering*, 2020, **8**, 9335-9345.
96. J. Xu, P. Zhu, I. H. El Azab, B. B. Xu, Z. Guo, A. Y. Elnaggar, G. A. Mersal, X. Liu, Y. Zhi and Z. Lin, *Chinese Journal of Chemical Engineering*, 2022.
97. H. Li, M. Liu, W. Zou, Y. Lv, Y. Liu and L. Chen, *ACS Sustainable Chemistry & Engineering*, 2022, **10**, 5430-5440.
98. P. Yan, M. M. J. Li, E. Kennedy, A. Adesina, G. Zhao, A. Setiawan and M. Stockenhuber, *Catalysis Science & Technology*, 2020, **10**, 810-825.
99. Y. Yang, C. Ochoa-Hernández, A. Víctor, P. Pizarro, J. M. Coronado and D. P. Serrano, *Applied Catalysis B: Environmental*, 2014, **145**, 91-100.
100. J. Van de Loosdrecht, A. Van Der Kraan, A. Van Dillen and J. Geus, *Journal of Catalysis*, 1997, **170**, 217-

226.
101. G. Neri, A. Visco, A. Donato, C. Milone, M. Malentacchi and G. Gubitosa, *Applied Catalysis A: General*, 1994, **110**, 49-59.
102. S. Velu, M. Kapoor, S. Inagaki and K. Suzuki, *Applied Catalysis A: General*, 2003, **245**, 317-331.
103. W. Song, Y. Liu, E. Baráth, C. Zhao and J. A. Lercher, *Green Chemistry*, 2015, **17**, 1204-1218.
104. Y. Chen, C. Liaw and L. Lee, *Applied Catalysis A: General*, 1999, **177**, 1-8.
105. C. Zhao, S. Kasakov, J. He and J. A. Lercher, *Journal of Catalysis*, 2012, **296**, 12-23.
106. P. M. Mortensen, J. D. Grunwaldt, P. A. Jensen and A. D. Jensen, *ACS Catalysis*, 2013, **3**, 1774-1785.
107. Y. Yang, G. Lv, L. Deng, B. Lu, J. Li, J. Zhang, J. Shi and S. Du, *Microporous and Mesoporous Materials*, 2017, **250**, 47-54.
108. R. Shu, R. Li, B. Lin, C. Wang, Z. Cheng and Y. Chen, *Biomass and bioenergy*, 2020, **132**, 105432.
109. Y. Yang, C. Ochoa-Hernández, P. Pizarro, A. Víctor, J. M. Coronado and D. P. Serrano, *Applied Catalysis B: Environmental*, 2016, **197**, 206-213.
110. P. M. de Souza, R. C. Rabelo-Neto, L. E. Borges, G. Jacobs, B. H. Davis, T. Sooknoi, D. E. Resasco and F. B. Noronha, *ACS Catalysis*, 2015, **5**, 1318-1329.
111. V. O. Gonçalves, C. Ciotonea, S. Arrii-Clacens, N. Guignard, C. Roudaut, J. Rousseau, J. M. Clacens, S. Royer and F. Richard, *Applied Catalysis B: Environmental*, 2017, **214**, 57-66.
112. F. Yang, D. Liu, H. Wang, X. Liu, J. Han, Q. Ge and X. Zhu, *Journal of Catalysis*, 2017, **349**, 84-97.
113. A. Robinson, G. A. Ferguson, J. R. Gallagher, S. Cheah, G. T. Beckham, J. A. Schaidle, J. E. Hensley and J. W. Medlin, *ACS Catalysis*, 2016, **6**, 4356-4368.
114. K. A. Resende, A. H. Braga, F. B. Noronha and C. E. Hori, *Applied Catalysis B: Environmental*, 2019, **245**, 100-113.
115. T. M. Sankaranarayanan, A. Berenguer, C. Ochoa-Hernández, I. Moreno, P. Jana, J. M. Coronado, D. P. Serrano and P. Pizarro, *Catalysis Today*, 2015, **243**, 163-172.
116. C. Tu, J. Chen, W. Li, H. Wang, K. Deng, V. A. Vinokurov and W. Huang, *Sustainable Energy & Fuels*, 2019, **3**, 3462-3472.
117. F. Broglia, L. Rimoldi, D. Meroni, S. De Vecchi, M. Morbidelli and S. Ardizzone, *Fuel*, 2019, **243**, 501-508.
118. D. Laurenti, P. Afanasiev and C. Geantet, *Applied Catalysis B: Environmental*, 2011, **101**, 239-245.
119. M. Lu, Y. Sun, P. Zhang, J. Zhu, M. Li, Y. Shan, J. Shen and C. Song, *Industrial & Engineering Chemistry Research*, 2019, **58**, 1513-1524.
120. F. Bouxin, X. Zhang, I. Kings, A. Lee, M. Simmons, K. Wilson and S. Jackson, *Applied Catalysis A: General*, 2017, **539**, 29-37.
121. J. Zhang, C. Li, X. Chen, W. Guan and C. Liang, *Catalysis Today*, 2019, **319**, 155-163.
122. N. T. Tran, Y. Uemura, S. Chowdhury and A. Ramli, *Applied Catalysis A: General*, 2016, **512**, 93-100.
123. W. Li, H. Wang, X. Wu, L. E. Betancourt, C. Tu, M. Liao, X. Cui, F. Li, J. Zheng and R. Li, *Fuel*, 2020, **274**, 117859.
124. R. Barton, M. Carrier, C. Segura, J. G. Fierro, S. Park, H. Lamb, N. Escalona and S. Peretti, *Applied Catalysis A: General*, 2018, **562**, 294-309.
125. W. Schutyser, S. Van den Bosch, J. Dijkmans, S. Turner, M. Meledina, G. Van Tendeloo, D. P. Debecker and B. F. Sels, *ChemSusChem*, 2015, **8**, 1805-1818.
126. W. Song, Y. He, S. Lai, W. Lai, X. Yi, W. Yang and X. Jiang, *Green Chemistry*, 2020, **22**, 1662-1670.

127. X. Zhang, P. Yan, B. Zhao, K. Liu, M. C. Kung, H. H. Kung, S. Chen and Z. C. Zhang, *ACS Catalysis*, 2019, **9**, 3551-3563.
128. M. Selvaraj, K. Shanthi, R. Maheswari and A. Ramanathan, *Energy & Fuels*, 2014, **28**, 2598-2607.
129. D. Raikwar, M. Munagala, S. Majumdar and D. Shee, *Catalysis Today*, 2019, **325**, 117-130.
130. H. Shafaghat, P. S. Rezaei and W. M. A. W. Daud, *Journal of Industrial and Engineering Chemistry*, 2016, **35**, 268-276.
131. J. Sun, A. M. Karim, H. Zhang, L. Kovarik, X. S. Li, A. J. Hensley, J. S. McEwen and Y. Wang, *Journal of Catalysis*, 2013, **306**, 47-57.
132. M. Liu, J. Zhang, L. Zheng, G. Fan, L. Yang and F. Li, *ACS Sustainable Chemistry & Engineering*, 2020, **8**, 6075-6089.
133. C. M. Pichler, D. Gu, H. Joshi and F. Schüth, *Journal of Catalysis*, 2018, **365**, 367-375.
134. Y. Wu, X. Xu, Y. Sun, E. Jiang, X. Fan, R. Tu and J. Wang, *Renewable Energy*, 2020, **152**, 1380-1390.
135. J. Qi, X. Sun, S. F. Tang, Y. Sun, C. Xu, X. Li and X. Li, *Applied Catalysis A: General*, 2017, **535**, 24-31.
136. A. Y. Bunch, X. Wang and U. S. Ozkan, *Journal of Molecular Catalysis A: Chemical*, 2007, **270**, 264-272.
137. D. Shen and S. Gu, *Bioresource technology*, 2009, **100**, 6496-6504.
138. Y. Román-Leshkov, C. J. Barrett, Z. Y. Liu and J. A. Dumesic, *Nature*, 2007, **447**, 982-985.
139. M. Przydacz, M. Jędrzejczyk, M. Brzezińska, J. Rogowski, N. Keller and A. M. Ruppert, *The Journal of Supercritical Fluids*, 2020, **163**, 104827.
140. S. Sitthisa and D. E. Resasco, *Catalysis Letters*, 2011, **141**, 784-791.
141. C. Zhu, H. Wang, H. Li, B. Cai, W. Lv, C. Cai, C. Wang, L. Yan, Q. Liu and L. Ma, *ACS Sustainable Chemistry & Engineering*, 2019, **7**, 19556-19569.
142. D. P. Duarte, R. Martínez and L. J. Hoyos, *Industrial & Engineering Chemistry Research*, 2016, **55**, 54-63.
143. J. Davis and M. Barteau, *Journal of the American Chemical Society*, 1989, **111**, 1782-1792.
144. R. Shekhar, M. A. Barteau, R. V. Plank and J. M. Vohs, *The Journal of Physical Chemistry B*, 1997, **101**, 7939-7951.
145. M. Mavrikakis and M. A. Barteau, *Journal of Molecular Catalysis A: Chemical*, 1998, **131**, 135-147.
146. M. A. Barteau, *Catalysis Letters*, 1991, **8**, 175-183.
147. M. S. Gyngazova, L. Negahdar, L. C. Blumenthal and R. Palkovits, *Chemical Engineering Science*, 2017, **173**, 455-464.
148. M. Y. Chen, C. B. Chen, B. Zada and Y. Fu, *Green Chemistry*, 2016, **18**, 3858-3866.
149. C. P. Jiménez-Gómez, J. A. Cecilia, C. García-Sancho, R. N. Moreno-Tost and P. Maireles-Torres, *ACS Sustainable Chemistry & Engineering*, 2019, **7**, 7676-7685.
150. N. Siddiqui, A. S. Roy, R. Goyal, R. Khatun, C. Pendem, A. N. Chokkapu, A. Bordoloi and R. Bal, *Sustainable Energy & Fuels*, 2018, **2**, 191-198.
151. N. Viar, J. M. Requies, I. Agirre, A. Iriondo, M. Gil-Calvo and P. L. Arias, *ACS Sustainable Chemistry & Engineering*, 2020, **8**, 11183-11193.
152. W. Li, G. Fan, L. Yang and F. Li, *Green Chemistry*, 2017, **19**, 4353-4363.
153. F. Tang, L. Wang, M. D. Walle, A. Mustapha and Y.-N. Liu, *Journal of Catalysis*, 2020, **383**, 172-180.
154. B. Seemala, C. M. Cai, C. E. Wyman and P. Christopher, *ACS Catalysis*, 2017, **7**, 4070-4082.
155. P. Wang, Y. Jing, Y. Guo, Y. Cui, S. Dai, X. Liu and Y. Wang, *Catalysis Science & Technology*, 2020, **10**, 4256-4263.

156. X. Kong, Y. Zhu, H. Zheng, Y. Zhu and Z. Fang, *ACS Sustainable Chemistry & Engineering*, 2017, **5**, 11280-11289.
157. S. Sitthisa, W. An and D. E. Resasco, *Journal of Catalysis*, 2011, **284**, 90-101.
158. W. Yu, K. Xiong, N. Ji, M. D. Porosoff and J. G. Chen, *Journal of Catalysis*, 2014, **317**, 253-262.
159. Z. Zhang, Z. Pei, H. Chen, K. Chen, Z. Hou, X. Lu, P. Ouyang and J. Fu, *Industrial & Engineering Chemistry Research*, 2018, **57**, 4225-4230.
160. K. Jeništová, I. Hachemi, P. Mäki-Arvela, N. Kumar, M. Peurla, L. Čapek, J. Wärnå and D. Y. Murzin, *Chemical Engineering Journal*, 2017, **316**, 401-409.
161. C. Miao, O. Marin-Flores, S. D. Davidson, T. Li, T. Dong, D. Gao, Y. Wang, M. Garcia-Pérez and S. Chen, *Fuel*, 2016, **166**, 302-308.
162. M. W. Schreiber, D. Rodriguez-Niño, O. Y. Gutiérrez and J. A. Lercher, *Catalysis Science & Technology*, 2016, **6**, 7976-7984.
163. H. Zuo, Q. Liu, T. Wang, L. Ma, Q. Zhang and Q. Zhang, *Energy & Fuels*, 2012, **26**, 3747-3755.
164. F. Feng, L. Wang, X. Zhang and Q. Wang, *Industrial & Engineering Chemistry Research*, 2019, **58**, 5432-5444.
165. F. Feng, X. Niu, L. Wang, X. Zhang and Q. Wang, *Microporous and Mesoporous Materials*, 2020, **291**, 109705.
166. S. Xing, P. Lv, J. Wang, J. Fu, P. Fan, L. Yang, G. Yang, Z. Yuan and Y. Chen, *Physical Chemistry Chemical Physics*, 2017, **19**, 2961-2973.
167. P. Kumar, S. K. Maity and D. Shee, *ACS Omega*, 2019, **4**, 2833-2843.
168. B. Peng, X. Yuan, C. Zhao and J. A. Lercher, *Journal of the American Chemical Society*, 2012, **134**, 9400-9405.
169. K. B. Baharudin, M. Arumugam, J. Hunns, A. F. Lee, E. Mayes, Y. H. Taufiq-Yap, K. Wilson and D. Derawi, *Catalysis Science & Technology*, 2019, **9**, 6673-6680.
170. I. Hachemi, K. Jeništová, P. Mäki-Arvela, N. Kumar, K. Eränen, J. Hemming and D. Y. Murzin, *Catalysis Science & Technology*, 2016, **6**, 1476-1487.
171. B. Ma, H. Cui, D. Wang, P. Wu and C. Zhao, *Nanoscale*, 2017, **9**, 5986-5995.
172. B. Ma, X. Yi, L. Chen, A. Zheng and C. Zhao, *Journal of Materials Chemistry A*, 2016, **4**, 11330-11341.
173. R. Kukushkin, O. Bulavchenko, V. Kaichev and V. Yakovlev, *Applied Catalysis B: Environmental*, 2015, **163**, 531-538.
174. A. Ramesh, P. Tamizhdurai, P. S. Krishnan, V. K. Ponnusamy, S. Sakthinathan and K. Shanthi, *Fuel*, 2020, **262**, 116494.
175. E. W. Qian, N. Chen and S. Gong, *Journal of Molecular Catalysis A: Chemical*, 2014, **387**, 76-85.
176. R. Loe, E. Santillan-Jimenez, T. Morgan, L. Sewell, Y. Ji, S. Jones, M. A. Isaacs, A. F. Lee and M. Crocker, *Applied Catalysis B: Environmental*, 2016, **191**, 147-156.
177. Z. Zhang, H. Chen, C. Wang, K. Chen, X. Lu, P. Ouyang and J. Fu, *Fuel*, 2018, **230**, 211-217.
178. Z. Zhang, Q. Yang, H. Chen, K. Chen, X. Lu, P. Ouyang, J. Fu and J. G. Chen, *Green Chemistry*, 2018, **20**, 197-205.
179. C. Miao, G. Zhou, S. Chen, H. Xie and X. Zhang, *Renewable Energy*, 2020, **153**, 1439-1454.
180. S. Leng, X. Wang, X. He, L. Liu, X. Zhong, G. Zhuang and J.-g. Wang, *Catalysis Communications*, 2013, **41**, 34-37.

181. E. Kordouli, B. Pawelec, K. Bourikas, C. Kordulis, J. L. G. Fierro and A. Lycourghiotis, *Applied Catalysis B: Environmental*, 2018, **229**, 139-154.
182. N. Chen, S. Gong and E. W. Qian, *Applied Catalysis B: Environmental*, 2015, **174**, 253-263.
183. X. Zhang, Q. Zhang, T. Wang, L. Ma, Y. Yu and L. Chen, *Bioresource technology*, 2013, **134**, 73-80.
184. X. Zhang, W. Tang, Q. Zhang, T. Wang and L. Ma, *Applied Energy*, 2018, **227**, 73-79.
185. T. Sankaranarayanan, M. Kreider, A. Berenguer, S. Gutiérrez-Rubio, I. Moreno, P. Pizarro, J. Coronado and D. Serrano, *Fuel*, 2018, **214**, 187-195.
186. G. C. Silva, D. Qian, R. Pace, O. Heintz, G. Caboche, E. Santillan-Jimenez and M. Crocker, *Catalysts*, 2020, **10**, 91.
187. E. Santillan-Jimenez, T. Morgan, R. Loe and M. Crocker, *Catalysis Today*, 2015, **258**, 284-293.
188. E. Santillan-Jimenez, R. Loe, M. Garrett, T. Morgan and M. Crocker, *Catalysis Today*, 2018, **302**, 261-271.
189. Q. Guo, M. Wu, K. Wang, L. Zhang and X. Xu, *Industrial & Engineering Chemistry Research*, 2015, **54**, 890-899.
190. T. Li, J. Cheng, R. Huang, J. Zhou and K. Cen, *Bioresource Technology*, 2015, **197**, 289-294.
191. S. Oh, H. S. Choi, I.-G. Choi and J. W. Choi, *RSC Advances*, 2017, **7**, 15116-15126.
192. H. Jahromi and F. A. Agblevor, *Applied Catalysis B: Environmental*, 2018, **236**, 1-12.
193. S. Cheng, L. Wei, J. Julson, K. Muthukumarappan and P. R. Kharel, *Fuel Processing Technology*, 2017, **167**, 117-126.
194. H. Jahromi and F. A. Agblevor, *Industrial & Engineering Chemistry Research*, 2018, **57**, 13257-13268.
195. S. Oh, J. H. Lee, I.-G. Choi and J. W. Choi, *Renewable Energy*, 2020, **149**, 1-10.
196. C. Zhao and J. A. Lercher, *Angewandte Chemie International Edition*, 2012, **51**, 5935-5940.
197. Y. Li, C. Zhang, Y. Liu, X. Hou, R. Zhang and X. Tang, *Energy & Fuels*, 2015, **29**, 1722-1728.
198. Y. Li, C. Zhang, Y. Liu, S. Tang, G. Chen, R. Zhang and X. Tang, *Fuel*, 2017, **189**, 23-31.
199. H. Lee, Y. M. Kim, K. B. Jung, J. Jae, S. C. Jung, J. K. Jeon and Y. K. Park, *Journal of Cleaner Production*, 2018, **174**, 763-770.
200. P. Arora, H. Abdolahi, Y. W. Cheah, M. A. Salam, E. L. Grennfelt, H. Rådberg, D. Creaser and L. Olsson, *Catalysis Today*, 2021, **367**, 28-42.
201. C. Boscagli, C. Yang, A. Welle, W. Wang, S. Behrens, K. Raffelt and J. D. Grunwaldt, *Applied Catalysis A: General*, 2017, **544**, 161-172.
202. P. M. Mortensen, D. Gardini, H. W. de Carvalho, C. D. Damsgaard, J. D. Grunwaldt, P. A. Jensen, J. B. Wagner and A. D. Jensen, *Catalysis Science & Technology*, 2014, **4**, 3672-3686.